Nanoscale

REVIEW

View Article Online
View Journal | View Issue

Cite this: *Nanoscale*, 2023, **15**, 16514

Enhancing electrochemical sensing through the use of functionalized graphene composites as nanozymes

Livia Alexandra Dinu[a] and Sevinc Kurbanoglu *[b]

Graphene-based nanozymes possess inherent nanomaterial properties that offer not only a simple substitute for enzymes but also a versatile platform capable of bonding with complex biochemical environments. The current review discusses the replacement of enzymes in developing biosensors with nanozymes. Functionalization of graphene-based materials with various nanoparticles can enhance their nanozymatic properties. Graphene oxide functionalization has been shown to yield graphene-based nanozymes that closely mimic several natural enzymes. This review provides an overview of the classification, current state-of-the-art development, synthesis routes, and types of functionalized graphene-based nanozymes for the design of electrochemical sensors. Furthermore, it includes a summary of the application of functionalized graphene-based nanozymes for constructing electrochemical sensors for pollutants, drugs, and various water and food samples. Challenges related to nanozymes as electrocatalytic materials are discussed, along with potential solutions and approaches for addressing these shortcomings.

Received 29th April 2023,
Accepted 15th August 2023

DOI: 10.1039/d3nr01998e

rsc.li/nanoscale

Introduction

In recent decades, electroanalytical techniques have been exploited to quickly detect toxic chemicals, pollutants, drugs, biologically important compounds, *etc.*, because they bring essential advantages, such as increased sensitivity, small costs, quick response period, and the possibility of on-site monitoring, through miniaturization.[1] As highly sensitive and selective analytical tools, electrochemical sensors are an outstanding choice. Enzyme-based sensors represent one of the most selective electrochemical sensors. However, they have several drawbacks, such as complex immobilization procedures (cross-linking and stabilizing reagents) that may cause loss of activity and signal reproducibility, special storage conditions (2–8 °C), low sensitivity, and reduced stability over time.[2] Also, they are losing ground in the progress toward a stable, reliable, sensitive, and selective sensing device for commercial use.[3] Likewise, cost-effectiveness is a another problem which can definitively affect sensor development because of the considerable large-scale implementation for environmental sensing needs. Low-cost materials, which also benefit from unique physicochemical properties, are nanosized materials.

The findings from 2007 [4] broke the conventional idea that inorganic materials are bio-inert, and inspired researchers to explore nanomaterials as catalysts or artificial enzymes called "nanozymes" in electrochemical applications. Recently, the nanozyme tag was announced as a term to embrace all nanosized materials with artificial enzymatic activity. The scientific area of nanozymes embodies an incipient research field, which has generated tremendous scientific enthusiasm due to nanozymes' superior properties in terms of 'refined' response to external incentives, self-assembly ability, large surface area, size-dependent catalytic activities and, most important, their structural tunability.[5]

Nanozymes are classified into two categories based on the reactions of the enzymes mimicked. The first is the nanozymes that mimic oxidoreductases (*e.g.*, glutathione oxidase, peroxidase, glucose oxidase, catalase, superoxide dismutase, nitrate reductase, *etc.*). The second one is the nanozymes that mimic hydrolase (*e.g.*, nuclease, esterase, phosphatase, protease, *etc.*).[6–10] The up-to-the-minute artificial enzymes are nanozymes, and they can be separated into four groups matching the type of material: metallic nanozymes (*e.g.*, silver, copper, gold, *etc.*),[11–13] metal–oxide nanozymes (*e.g.*, cerium or ferric oxide), carbon-related nanozymes (*e.g.*, functionalized graphene or graphene quantum dots)[14–17] and other 2D nanomaterials.[5,18,19] These nanozymes were described as oxidoreductase-mimicking materials (*e.g.*, laccase, horseradish peroxidase), hydrolases, and lyases such as phosphatase or

[a]*National Institute for Research and Development in Microtechnologies (IMT Bucharest), 126A Erou Iancu Nicolae Street, 077190 Voluntari, Ilfov, Romania*
[b]*Faculty of Pharmacy, Department of Analytical Chemistry, Ankara University, 06560, Tandogan, Ankara, Türkiye. E-mail: skurbanoglu@gmail.com*

anhydrase, respectively.[20] The tunability is simply adjustable by varying the elements, dimensions, surface properties, and morphology of the dots.[21] The exceptional chemical and physical properties of nanomaterials allow endless functionalization and modification that easily generates nanozyme materials. With the fast expansion and ongoing development of modern technology, nanozyme materials offer several benefits such as increased catalytic response due to the high stability of the nanomaterial, facile route to functionalization, and lower costs for the synthesis of nanomaterials than the synthesis of biomaterials (enzymes). Moreover, nanozymes have found extensive application in biosensors[22–25] to enhance signal conduction and enhance the sensitivity of detection. By leveraging these advantages, nanozymes contribute to improved determination sensitivity, making them valuable components in the development of sensing technologies.[26]

The family of carbon nanomaterials, such as graphene and its derivatives,[27–29] fullerene,[30] and carbon nanotubes,[31] has been intensively studied as enzyme-mimicking materials in sensing and biosensing systems. The attention paid to applying functionalized graphene as nanozymes for the development of sensors is owing to the advantages, such as enhanced electron-transfer kinetics, easy functionalization, high stability, low costs, and biocompatibility, associated with their unique morphologies. However, there is still considerable space to advance the catalytic aptitude of graphenic nanozymes. Modifying the graphene surface with metallic and bimetallic nanoparticles can improve its nanozymatic features. In this context, the functionalization of graphene oxide envisages graphene-based nanozymes that act as perfect candidates for copying the active site microenvironment of several natural enzymes. Fig. 1 illustrates the variety of graphene-based derivatives, their 3D-structured composites, and the various functionalization groups employed in the development of nanozyme materials. This comprehensive representation highlights the diverse range of approaches utilized to harness the potential of graphene in creating nanozymes for various applications.

Livia Alexandra Dinu

Dr Livia Dinu graduated from the Faculty of Chemistry, University of Bucharest, in 2010. In 2012 she got her master's degree from the same university, with the thesis "DNA-based biosensors for the detection of neurotransmitters in biological samples". She received her Ph.D. degree in Chemistry (2015), from the Faculty of Applied Chemistry and Materials Science at the University Politehnica of Bucharest. The thesis was focused on developing electrochemical platforms that used nanosized materials for the detection of obesity biomarkers from biological samples. In 2015 she was a visiting researcher at Ruhr University, in Bochum, Germany, in Prof. Dr Wolfgang Schumann's Laboratory. In September 2016, Dr Livia Dinu received the "Constantin Luca" medal and award for the best young analytical chemist for excellence in research, awarded by the Romanian International Chapter of the ACS. Dr Dinu is currently a second-degree researcher at the National Institute for Research and Development for Microtechnologies, IMT-Bucharest, Romania. In the last four years, she has investigated nanozyme type of materials as sensing materials in the development of electrochemical sensors.

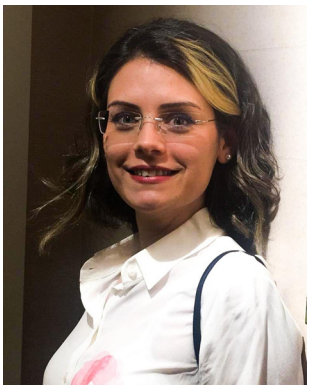

Sevinc Kurbanoglu

Dr Sevinc Kurbanoglu is currently an Associate Professor at the Ankara University Faculty of Pharmacy, Department of Analytical Chemistry, in Turkey. She graduated from the Middle East Technical University, Ankara, in 2008. She got her master's degree from the same university, with the topic of conducting polymer-based electrochemical biosensors. She studied in Prof. Dr Lo Gorton's Laboratory at Lund University, Sweden, as visiting researcher, during her master's studies. She received her Ph.D. degree in Analytical Chemistry from the Pharmacy Faculty of Ankara University in 2016 under the supervision of Prof. Sibel A. Ozkan. Moreover, she was also a visiting researcher during her Ph.D. at Prof. Dr Arben Merkoçi's Laboratory at Barcelona Autonoma University, Catalan Nanoscience and Nanotechnology Institute. Related to her Ph.D. thesis topic, she conducted research about tyrosinase inhibition through drugs and pesticides. For postdoctoral studies, she was in collaboration with Prof. Dr Frieder W. Scheller about molecularly imprinted polymers for drug analyses in the Department of Analytical Biochemistry at Potsdam University. She has published over 80 manuscripts in peer-reviewed journals and 25 book chapters. She was awarded the Outstanding Success Award from the Presidency of Higher Education Council of Turkey, as the best Ph. D. Thesis in 2017 and additionally a Biosensor 2021 Early-Career Women Award. Her research interests include biosensors, biological and chemical nanosensors, enzyme-based nanobiosensors, DNA-based nanosensors, electrochemical assays for pharmaceutical compounds, validation, and electrochemical sensors.

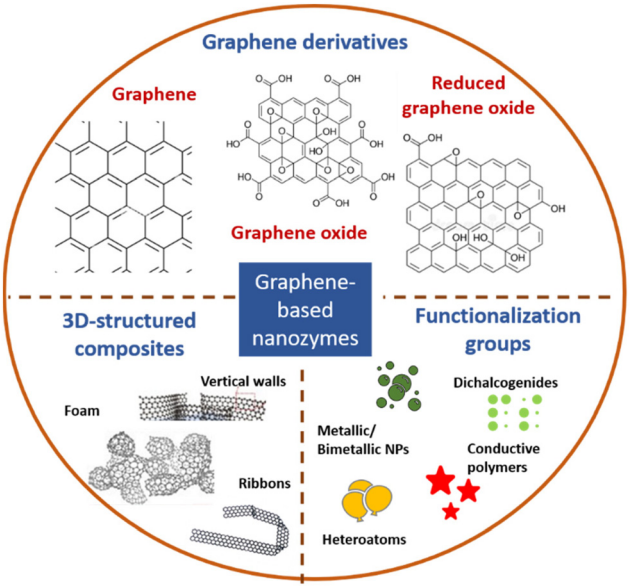

Fig. 1 Different categories of artificial enzymes (nanozymes) according to the type of graphene derivative.

Taking cues from nature by studying the structure of the natural enzymes, researchers considered that metal nanoparticles would bring unprecedented sensitivity to the graphene-based nanozymes, not only due to their high ability to transfer electrons at the electrode–solution interface but also due to the fact that it recreates the active center of the enzyme: such as iron-containing heme, the natural active site of horseradish peroxidase, or copper as the active center of laccase enzyme. The immobilization of metallic or bimetallic nanoparticles on top of graphene material to imitate the natural enzymatic microenvironment has empowered researchers worldwide to develop highly sensitive and selective sensors. Moreover, graphene-based nanozymes benefit from the intrinsic properties of the nanosized material, offering a more stable substitute for enzymes and a multiplex framework for investigating sophisticated biochemical reactions. The great expectation of this research is to be able to replace enzymes through the development of enzyme-based biosensors with nanozymes.

This review provides a concise overview of the synthesis methods employed for various nanocomposites and functionalized nanomaterials derived from graphene, including simple graphene (GR), oxidized graphene (GO), reduced graphene (rGO), and architectural forms of graphene. Each subsection delves into the development of electrochemical sensors using these innovative graphene nanozymes, elucidating their analytical capabilities. Throughout the review, we only focus on graphene-related materials.

Synthesis routes of nanozymes

Nanosized materials exhibit various nanozymatic features also due to the route of synthesis. Different synthesis routes and precursors can bring unexpected catalytic properties to similar nanomaterials. There are a large number of methods[32] (Fig. 2) for the preparation of nanosized materials with nanozymatic characteristics, such as hydrothermal and solvothermal methods, co-precipitation, electrochemical and sol–gel methods.

Graphene oxide was first prepared by Brodie *et al.* in 1859 by different methods such as the Staudenmaier method, the Hofmann method and the Hummers method. The Hummers method, which uses safe, low-toxicity chemicals and saves time, was developed by Hummers and Offeman in 1958. Unlike the traditional Hummers method, the modified Hummers method, which does not contain $NaNO_3$, has been reported as an advantageous method in terms of preventing toxic gas release.[33,34] Graphene oxide is typically synthesized using the Hummers method, and subsequently, reduced graphene oxide can be synthesized through a straightforward hydrothermal approach. The extent of reduction is usually influenced by temperature, with higher temperatures facilitating a faster reduction of graphene oxide.[35,36]

The most studied graphene nanozymes are based on nanocomposite formation using metallic and bimetallic nanoparticles. Metallic and bimetallic graphene nanozymes can be synthesized in the same synthesis step, but they can also be synthesized separately and self-assembled on top of the electrochemical transducer. Some synthesis methods used to obtain individual metallic and bimetallic nanozymes are preformed-seed-mediated growth (PSMG),[37] the high-temperature reduction method,[38–40] electrochemical synthesis, photochemical processes, and biosynthesis.[41] With different methods, various forms of metallic and bimetallic nanoparticles (*e.g.*, nanoparticles,[12,42] nanoclusters,[43] nanorods,[44] nanosheets[12]) can be obtained. The PSMG method is practicable for controlling the size by varying the concentration and type of seeds in the growth precursor solution.[45]

In the literature, there exist some review papers discussing nanozymes, highlighting the research progress of nanozymes in particular fields,[3,46,47] or for sensing applications in general,[48] or commenting on the working mechanism[49] of specific enzymes. The following section will present a short description

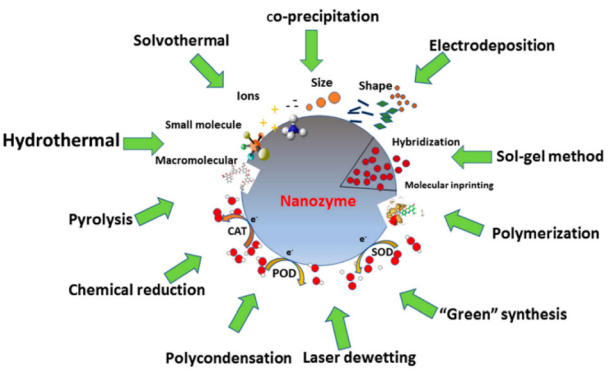

Fig. 2 Principal scheme of the methods for nanocatalyst synthesis (reprinted from ref. 32, with permission from MDPI Publisher).

of the synthesis routes for several nanocomposites and functionalized nanomaterials based on simple graphene (GR), but also the oxidized form (GO), reduced form (rGO), and architectural form of GR. In each subsection, the design of electrochemical sensors using these novel graphene nanozymes and their analytical performances are discussed.

Applications of functionalized graphene derivatives as nanozymes for electrochemical sensing

Graphene composites as nanozymes for electrochemical sensing

Graphene, a 2D carbon-based material with excellent conductivity and a large active area, is the most studied nanomaterial in various fields, especially in electrochemical sensing and biosensing.[50] In the following section, GR nanozyme materials exploited to shape electrochemical sensing devices (glassy carbon and screen printed electrodes, GCE and SPE) are described for the analysis of hydrogen peroxide (H_2O_2),[51,52] catechol (CAT),[53–55] hydroquinone (HQ),[53–57] and cholesterol,[58] and summarized in Table 1.

H_2O_2 is the leading secondary product of numerous oxidative metabolic routes. H_2O_2 was identified as a significant controller of eukaryotic responses, produced in reply to numerous internal and external stimuli that include cytokines, interleukins, and growth factors.[61] The connection between H_2O_2 levels and human health has drawn significant interest, and the determination of H_2O_2 has become of fundamental significance in environmental and industrial fields, and in clinical and biochemical research areas. In 2014, a GCE was functionalized using gold nanorods and GR (GR–AuNRs) for the nonenzymatic detection of H_2O_2 from milk samples[51] (Fig. 3). First, the GO was synthesized by the Hummers classic recipe, followed by a reduction process to obtain the graphene material. Second, the AuNRs were synthesized using the method of seed-mediated growth by mixing cetyltrimethylammonium bromide (CTAB) and chloroauric acid ($HAuCl_4$) with sodium \borohydride ($NaBH_4$). GR–AuNRs (1 mg mL^{-1}) suspension was obtained by mixing the two nanomaterials in water and drop-cast on top of a clean GCE. A TEM image of the composite showed the presence of AuNR between the graphene layers and an agglomeration of AuNRs. The electrochemical system was formed from a three-electrode cell as follows: the prepared GR–AuNRs as WE, Ag/AgCl for RE, and Pt wire as CE. The proposed method showed linearity at the concentration level of

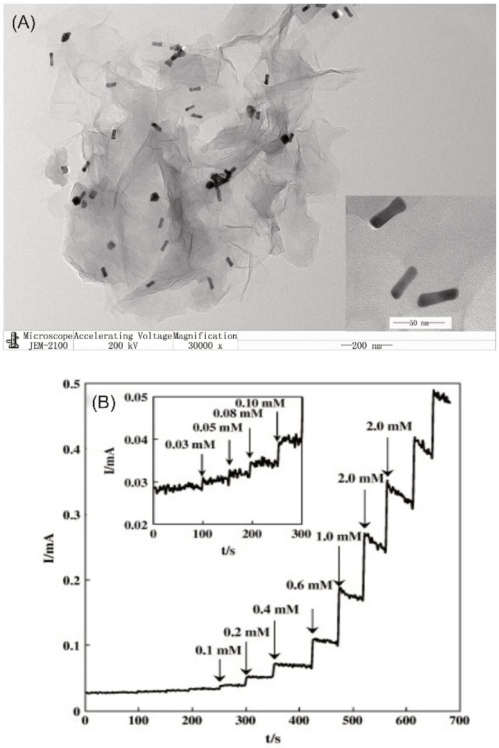

Fig. 3 (a) HRTEM image of GR–AuNRs. Inset shows magnified TEM images of AuNRs; (b) typical steady-state response of the GR–AuNRs/GCE to successive injection of H_2O_2 into the stirred N_2-saturated PBS (0.1 M, pH 9.0) (reprinted from ref. 51, with permission from Elsevier).

Table 1 Some selected graphene composites as nanozymes for electrochemical sensing

Nanozymes	Substrate	Method	Transducer	Medium	Linear range	LOD	Application	Ref.
Gr–AuNRs	H_2O_2	AMP	GCE	0.1 M PBS (pH 9.0)	30–5000 μM	10 μM	Milk	51
PtAu NPs–CTAB–Gr	H_2O_2	AMP	GCE	0.2 M PBS (pH 7.0)	0.005–4.8 μM	0.0017 μM	Human serum	52
CdTe QDs/Gr	CAT	DPV	GCE	PBS (pH 6.0)	30–1000 μM	0.09 μM	Industrial, lake, and surface water	54
Graphene-like carbon nanosheets	CAT	DPV	GCE	0.1 M PBS (pH 7.0)	0.5–50 μM	0.05 μM	Tap water and Xiangjiang River water	55
Gr-COOH	HQ	AdSV	GCE	0.05 M H_2SO_4 in 60 : 40 methanol: water	0.1–40 μM	0.04 μM	Whitening cosmetics	56
Gr/Ir(III)	HQ	DPV	GCE	1 M PBS (pH 7.2)	0.05–100 μM	0.0011 μM	Tap, lake, and river water	57
MnO_2/Gr	Cholesterol	DPV	PG	PBS (pH 7.0)	0.0012–0.024 μM	0.00042 μM	Human serum	58
MWCNTs-PDDA-Gr	CAT HQ	DPV	GCE	0.2 M PBS (pH 7.0)	0.5–400 μM	0.018 μM 0.02 μM	Tap water and seawater	59
AuNPs/N-doped nanoperforated Gr	H_2O_2	NA	GCE	NA	0.5–10 μM	0.5 μM	NA	60

3.0×10^{-5} M to 5.0×10^{-3} M, showing a sensitivity of 389.21 μA mM^{-1} cm^{-2}, and the LOD was calculated to be 0.1 nM, as also shown in Table 1. As potential interfering compounds, glucose, citric acid (CA), AA, tartaric acid (TA), and oxalic acid (OA) were investigated, and the recorded response was negligible compared with the response of the sensor for measuring H_2O_2. Using the standard addition method, the GR–AuNRs/GCE was useful for the detection of H_2O_2 in real milk samples, with a recovery percentage between 96.8 and 99.1%.

The phenol derivatives HQ, CAT, and resorcinol (RC) are dihydroxybenzene isomers with similar properties and structures, which generally cohabit and are exploited as crude and artificial intermediates in several industries such as the cosmetics, pharmaceutical, and pesticide fields. Therefore, the simultaneous and precise determination of at least two of these compounds is of great interest.[59] However, due to similarity in structure, HQ, CAT, and RC interfere with each other during their qualitative detection, making it challenging to determine these isomers together.[53] Song and coworkers[59] developed an electrochemical sensor for the concurrent detection of CAT and HQ from real samples collected from the environment or household areas, using a hybrid material based on GR functionalized with MWCNTs and poly(diallyldimethylammonium chloride) (PDDA). PDDA is a polyelectrolyte that is soluble in aqueous media, where it is positively charged. The interaction of PDDA and graphene was electrostatic and prevented GR from aggregation. A larger specific area was provided, in this paper, by combining the GR, which is a 2D nanomaterial, with MWCNTs, a 1D-structured nanomaterial. The hybrid material was obtained by adding 10 μL of PDDA (20%) to the homogeneous mixture of MWCNTs-GR.

The electrochemical cell was formed from 3 electrodes: the prepared hybrid material was drop-cast on GCE to form the WE, denoted PDDA-MWCNTs-GR/GCE, SCE was the RE, and a Pt wire was the CE. The PDDA-MWCNTs-GR/GCE was engaged for the concurrent detection of HQ and CAT, obtaining a linear concentration range from 0.5 to 400.0 μM for both isomers, with a calculated LOD of 0.018 μM for CAT and 0.02 μM for HQ, as summarized in Table 1. With the increase of pH, electrostatic repulsion between the anions occurred, and the separation was obtained with high current intensity at pH 7.0. The selectivity studies showed a very good tolerance as 1000-fold increased levels of Na^+, NH_4^+, K^+, Mg^{2+}, Ca^{2+}, Zn^{2+}, Cu^{2+}, Al^{3+}, SO_4^{2-}, NO_3, and 100-fold concentrations of AA, Fe^{3+}, UA, Ph or RC had no effects on the detection signals of HQ and CC (RSD $\leq$ 5%). The detection of CAT and HQ from water samples was done by using the standard addition method (SAM). The recovery percentages were 96.0–104.4% and 96.1–104.3% for CAT and HQ, respectively, showing very good results for the developed method.

Liu and coworkers[52] developed bimetallic PtAuNPs anchored on the surfactant – cetyl trimethyl ammonium bromide (CTAB) intercalated with graphene, for H_2O_2 detection from real samples. The GO was obtained by a modified Hummers method, while the PtAuNPs-CTAB-GR nanocomposite was synthesized by a synthetic hydrothermal strategy as follows: first, the GO and CTAB were dispersed in water and ultrasonicated for 4 h to obtain a suspension. After that, CTAB–GO was mixed with Pt and Au precursors, H_2PtCl_6 and $HAuCl_4$, respectively. A volume of 10 μL of obtained PtAuNPs–CTAB–GO composite was drop cast on top of GCE and left to dry in air. This proposed sensor showed very good electrochemical characteristics in comparison with bare GCE, CTAB–GO/GCE, AuNPs-CTAB-GR/GCE, and PtNPs-CTAB-GR/GCE, showing higher current intensity and demonstrating that CTAB could diminish the agglomeration of graphene layers, owing also to the superior conductivity provided by the bimetallic nanoparticles. The developed sensor showed good catalytic activity toward H_2O_2 and achieved a wide linear concentration range from 5.0 nM to 4.8 μM, with a LOD of 1.7 nM (S/N = 3). In evaluating the selectivity of the PtAuNPs-functionalized graphene electrode, no observable modification of the current intensities was observed when AA and UA were supplemented into the H_2O_2 solution. The feasibility of the sensor for real-world purposes was evaluated by investigating human serum samples, with recovery percentages of 96.8% and 106.4%.

In 2016,[54] a cadmium telluride QDs (CdTe QDs)-functionalized graphene was designed to modify the surface of a GCE for the detection of CAT through the increased catalytic action of the CdTe QDs. The CdTe QDs were synthesized using the hydrothermal method, and GO using a technique starting from the Hummers method. For the modification of GCE with GO, an electrodeposition step took place using CV at −1.4 to 0.6 V to obtain the GR/GCE, which was left to dry at room temperature. On top of the GR/GCE, 7 μL of CdTeQDs were dropped on the surface and dried with an IR lamp. The coated GCE was stored in double-distilled water, and it was stable for several weeks. The recorded current for the determination of different concentrations of CAT was linear in the range of 30–1000 μM, with a calculated LOD of 0.09 μM. Several possible interfering species were investigated. The study showed that no interference was observed for 100-fold K^+, Fe^{3+}, Na^+, Ca^{2+}, Al^{3+}, Mg^{2+}, SO_4^{2-}, NO_3^-, Cl^-, the 50-fold concentration of AA, glucose, and 20-fold BPA, RC, glutamic acid, and HQ. The applicability of the CdTe QDs-GR/GCE was investigated by measuring the CAT levels from spiked industrial and lake water gathered from a Chinese university and spiked surface water samples gathered from the Sichuan region. The recovery rates were between 98.3 and 104.3%, which showed that the projected sensor is reliable for CAT determination in water samples.

Carbon nanosheets similar to graphene (GCN) were reported[55] as a new nanomaterial in the design of working electrodes for the electrochemical detection of HQ and CAT. This GCN was synthesized from maltose using NH_4Cl and Co $(NO_3)_2$ as graphitization catalytic compounds. Interrelated C scaffolds with macropores were highlighted after performing the morpho-characterization, and their size was of a few hundred μm. Clearly, the porous carbon contained organized nanosheets. This graphitized material was further used to modify the working area of a GCE by the drop-casting technique and showed better analytical performances than GO and rGO. The GCN-based electrode was employed for the analysis

of CAT and HQ, having a linear response between levels of concentrations of 0.5 to 50 μM and 0.1–30 μM, respectively. The LOD values were 0.05 μM for HQ and 0.02 μM for CAT. When stored in pH 7 PB saline solution in the fridge for one month, the GCN/GCE showed 97% of its initial current signal, proving great storage stability. The I_p densities of HQ and CC showed no clear modification in the presence of a 100-fold level of Na^+, Ca^{2+}, Fe^{3+}, Mg^{2+}, Cl^-, NO^{3-}, $SO_4{}^{2-}$ and 10-fold level of nitrophenol, glucose, RC, phenol, and AA. To assess the application prospects of the GCN nanomaterial, tap and Xiangjiang river water were spiked with HQ and CAT and tested, with recovery percentages between 97.2% and 103%.

Cholesterol (Ch) is an essential compound in the human body, synthesized in the liver depending on the intake of healthy fats.[62] Ch has a crucial part in the synthesis of sex hormones, bile acids, and vitamins. It is a representative compound of the family of fatty alcohols, which are vital constituents of nerve and brain cells.[63] Increased levels of Ch in the blood occur because of the change of its ordinary equilibrium in the body, causing various cardiovascular diseases, cerebral thrombosis, and atherosclerotic disorders.[64]

In another study, a pencil graphite electrode (PGE)[58] was functionalized with GR functionalized with MnO_2 for the determination of Ch from serum samples. The geometric area of the PG is high, 0.65 cm^2, compared with GCE or SPE. GR was synthesized by a chemical technique, and a homogeneous paste was formed by mixing with the polymer polyvinylidene fluoride (PVDF). GR/PGE was obtained by brushing the formed graphene coating on the surface of the electrode. On top of GR/PGE, the MnO_2 was electrodeposited by CV from −1.0 V to 0.8 V from an acidic solution of $KMnO_4$, used as a precursor. The RE employed for the three-electrode cell used in this study was the SCE. The MnO_2/GR/PGE was further investigated using DPV to evaluate the critical parameters, and the detection of Ch linearity was observed in the concentration range of 1.1–24.0 nM, with a LOD value ($3\sigma/S$) of 0.42 nM. The sensitivity value of 63 869 μA μM^{-1} cm^{-2} was obtained for this sensor. The obtained results also showed great reproducibility and stability for a month-period of time. The compounds K^+, Mg^{2+}, Na^+, and Cl^- showed no interference in the Ch electrochemical response even in high concentrations of interferent. Glu and Gly were similarly tested, and the Ch analysis was possible when more than 200-fold and 300-fold concentrations, respectively, were present in the sample. The recovery values of Ch from spiked human blood serum were in the range of 99.2% to 100%.

In 2020, a GR functionalized with COOH groups (GR-COOH) was used to modify a GCE[56] to develop a sensor used to determine the ultra-sensitivity of HQ in drug samples. The response of the developed sensors was three, seven, and ten times increased compared with that of the GR/GCE, GCE-COOH, and bare GCE, respectively. The GR-COOH acted as an adsorbent material, ensuring that HQ molecules were adsorbed on the WE area. As a consequence, the sensitivity was increased, and the LOD was lower. For the HQ sensor, first, Gr was functionalized with $COOH^-$ by a carboxylation process and then added to GCE (diameter 3 mm) to form the Gr-COOH/GCE. The adsorption behavior of HQ was investigated using the proposed sensor by AdSV, and a linear concentration range was reported between 0.1 and 40 μM, and a LOD value of 0.04 μM. Six freshly prepared electrodes were tested, and no significant differences in sensitivity were observed, confirming the excellent repeatability of the preparation. The effects of 50-fold phenol, 2-nitrophenol, and 100-fold of glucose, Ca^{2+}, Mg^{2+}, Zn^{2+}, Fe^{2+}, K^+, Na^+, Cl^-, $SO_4{}^{2-}$, $CO_3{}^{2-}$ and $NO_3{}^-$ produced differences in the current response less than five when evaluating 40 μM HQ. To test the applicability, fifteen cosmetic samples were investigated, and the concentration of HQ obtained using the Gr-COOH/GCE was in very good correlation with the UV-derivative standard spectrophotometric method, indicating that the proposed sensor could be employed to assess HQ in skin-lightening products.

In recent studies, transitional metals (TM) have attracted great interest. One of the most intensively studied 6d-TM is iridium (Ir) complexes. Typically, Ir(III) complex containing 2-phenylpyridine has been identified for exploitation in several optical applications[65] due to its optical characteristics. Unexpectedly, Miao and collaborators[66] discovered, in 2016, that Ir(III) complex also benefits from high conductive properties, and his group developed a label-free and nonenzymatic electrochemical device to detect H_2O_2 based on a new switch system using an Ir(III) complex and methylene blue (MB) as a mediator to quicken the electron transfer and AuNPs to intensify the electrochemical response.

In 2020, Mohd Yazid and coworkers[57] developed an HQ sensor by modifying a GCE with a GR/iridium(III) dimer complex composite to obtain the GR/Ir(III) complex electrode. The GR and a dichlorobridged Ir(III) dimer were synthesized separately using methods already reported in the literature and briefly presented by the authors. The classical drop-casting technique was applied for the design of the GCE modified with the GR/Ir(III) complex. Only 1.5 μL was used to form a uniform film on top of the GCE, and left to dry at 24 °C, using a beaker placed on top of the electrode. Under optimum conditions, SW voltammograms were recorded, and HQ was detected in the concentration ranges of 1.5–100 μM and 0.05–1.5 μM with good sensitivity of 1120.64 μA mM^{-1} cm^{-2} and a value of LOD of 1.1 nM (S/N = 3). During the interference studies, the signal responses were <7%, signifying a good tolerance of the proposed sensor for the detection of HQ in the presence of Me^+ that are regularly present in water, such as Cu^{2+}, Cd^{2+}, Na^+, Ba^{2+}, K^+, Hg^+, Ag^+, Pb^{2+}, Mg^{2+}, Al^{3+}, and Cr^{3+}. The analytical applications were investigated by testing the proposed GR/Ir(III) complex electrode in tap, lake, and river water samples, all collected from Perak, Malaysia. The obtained recoveries ranged from 98.4% to 102.9%, with an RSD value lower than 3.1%.

Graphene oxide composites as nanozymes for electrochemical sensing

Graphene oxide (GO), an intensively studied graphene derivative, is typically formed by the chemical exfoliation of graphitic

rods by strong oxidizing reagents. The GO contains, in its structure, numerous functional groups, such as e and epoxy group; also –COOH, –C═O, C_6H_6-OH, and a few others in smaller proportions, by the edges of GO.[67] Related to GR, the presence of all oxygenated groups in GO disturbs its physicochemical properties.[68,69] Taking into consideration these aspects, GO is an interesting substrate material for the formation of nanozyme-based electrochemical sensing applications. In the next section, GO-based nanozyme materials used for shaping electrochemical sensors are described for the analysis of H_2O_2,[70–73] HQ,[74,75] sialic acid,[76] carbofuran, and carbaryl,[77] catechol,[75,78,79] or urea,[80] and summarized in Table 2.

In 2015, Erogul and coworkers[75] functionalized graphene oxide with APTES-coated Fe_3O_4 nanoparticles by mixing with EDC as an activating agent and then adding AuNPs. The design of the proposed electrochemical sensor, denoted AuNPs/Fe_3O_4-APTES-GO, took place in two steps. First, the suspension Fe_3O_4-APTES-GO (prepared in 0.5% chitosan) was drop cast on top of a GCE, followed by the electrodeposition at −0.2 V for 180 s of AuNPs from a solution of $HAuCl_4$. Using the AuNPs/Fe_3O_4-APTES-GO/GCE, the oxidation potential difference was 120 mV, higher than 100 mV for the MWCNTs-PDDA-GR/GCE described above, meaning that by using metallic nanoparticles the separation between the two isomers could be better discriminated. The linear concentration range for HQ was 3–137 μM and for CAT was 2–145 μM, and the LOD values were 1.1 μM (HQ) and 0.8 μM (CAT). The storage stability of the developed GCE was effective for 23 days, and after nine working days, the signal was around 82% of its initial value. No interference in the recorded signal was observed when several organic and inorganic compounds (Ph, glucose, RC, DA, H_2O_2, $MgCl_2$, NaCl, $Zn(NO_3)_2$, and $CaCl_2$), were added to CAT and HQ solution. Real samples were prepared using the mentioned protocol, obtaining recovery percentages of 97.5–100.7% and 96.5–99% for CAT and HQ, respectively.

In another study, the composite of GO@polydopamine (GO@PDA) was decorated with AuNPs and deposited on top of a GCE for the detection of CAT from water samples.[81] The GO-PDA composite was prepared from graphite oxide under sonication, followed by the addition of DA under stirring, and left for 2 h for self-polymerization of DA on GO. After it was dried in an air oven, the resulting powder was redispersed in water, and 8 μL was deposited *via* the drop-casting technique onto the GCE. The AuNPs were electrochemically deposited on the composite surface by electrochemical deposition, in a potential range from 1.5 to −2.0 V starting from K($AuCl_4$) as the gold precursor in the H_2SO_4 solution. When not involved in measurement, all electrodes were stored at 24 °C in dry conditions. Considering the optimal parameters, the current signal of CAT at GO@PDA-AuNPs/GCE was linear in the concentration range of 0.3 to 67.55 μM with the LOD of 0.015×10^{-6} M, as also summarized in Table 2. The sensitivity of the sensor was the slope of the calibration curve: 4.66 ± 0.15 μA μM^{-1} cm^2. The addition of 100-fold of epinephrine (EP), AA, norepinephrine (NE), and 50-fold addition of HQ did not disturb the signal of the GO@PDA-AuNPs/GCE for detection of 1 μM of CAT. Tap water samples were spiked with CAT and investigated using the developed sensor, showing recovery rates from 96.0 to 97.5%.

Due to its very good analytical performance for H_2O_2 reduction, Prussian blue (PB) was introduced as a nanozyme that mimics the activity of peroxidase.[82] However, the electrochemical activity of PB was obstructed by its poor e^- transfer ability.[83] Hence, harmonizing the increased catalytic activity and the low conductivity of PB is an issue that can be overcome by adding a highly conductive nanomaterial that will help to obtain a better electrochemical performance of the sensors.

Since the first covalent organic frameworks (COFs) were reported in 2005, they have gained huge interest because they possess uniform porosity and a structure with precise period-

Table 2 Some selected graphene oxide composites as nanozymes for electrochemical sensing

Nanozymes	Substrate	Method	Transducer	Medium	Linear range	LOD	Application	Ref.
GO–PAMAM–Fe^{2+}	H_2O_2	DPV	GCE	1 M ABS (pH 4.3)	0.5–2000 μM	0.18 μM	Milk, fetal bovine serum	70
L-Cys-Ag(I) Cp/GO	H_2O_2	AMP	GCE	0.1 M PBS (pH 7.0)	1–5000 μM	0.3 μM	Human serum and human urine	71
Nafion/GO-AuNP	H_2O_2	DPV	ITO	Potassium hydrogen phthalate and sodium azide (pH 4.0)	0.01–10 000 μM	1.9×10^{-3} μM	NS	72
AuNPs/PB/GO	H_2O_2	AMP	GCE	0.5 M KCl (pH 3.0)	3.8–5400 μM	1.3 μM	NS	73
PN-COFs /GO	HQ	DPV	GCE	PBS (pH 6.0)	0.1–100 μM	0.009 μM	Whitening cream	74
AuNPs/Fe_3O_4-APTES-GO	HQ CAT	AMP	GCE	0.1 M PBS (pH 7.4)	3–137 μM 2–145 μM	1.1 μM 0.8 μM	Tap water	75
FPBA-DA/TCPP-GO	Sialic acid	DPV	GCE	PBS (pH 7.4)	100–7500 μM	28.5 μM	Human blood and urine	76
MIL(Fe)-101 MOFs@GO	Carbofuran Carbaryl	DPV	GCE	BRB (pH 4.0)	0.005–0.2 μM 0.001–0.3 μM	0.0012 μM 0.0005 μM	Cucumbers, oranges, tomatoes, and cabbage	77
$NiMoO_4$ @ GO	CAT	LSV	SPCE	0.1 M PBS (pH 7.0)	0.01–273 μM	0.0015 μM	Industrial, domestic, and underground water	79
NiS/GO	Urea	DPV	GCE	1 M KOH	100–1000 μM	3.79 μM	Milk	80
GO@PDA-AuNPs	CAT	DPV	GCE	0.1 M PBS (pH 7.0)	0.3–67.55 μM	0.015 μM	Tap water	81

icity.[84] The COFs are categorized as 2 or 3D scaffolds. The 2D benefit from higher mobility for the charged molecules due to nanoporous space between layers, and for this reason they act as very good materials in the expansion of nanozyme-based sensors.[84]

In 2020, Ma *et al.*[74] projected a GO modification with a new porphyrin-based COF material (PN-COFs) to investigate the detection of HQ and AC. Acetaminophen (AC) is a broadly active medication that has been used for pain and fever for several years.[85] Unnecessary intake of AC may cause deposits to form on the liver, causing damage to this organ.[86] Regularly, AC is obtained by direct amidation of HQ. In this study, the investigated porphyrin was synthesized by taking advantage of the imidization reaction between the tetraminophenyl porphyrin (TAPP) and 1,4,5,8-naphthalenetetracarboxylic dianhydride (NTCDA), using a modified solvothermal method, and the final product was dispersed in dimethylformamide (DMF). GO prepared by the Hummers method was distributed in water. Both were mixed until a suspension was created and drop cast on the GCE. Finally, the modified electrode was reduced by CVs in buffer solution from 0.60 V to −1.50 V. The prepared sensor was able to identify both analytes, HQ and AC, as the oxidation occurred with a peak potential separation of 30 mV. Under optimal parameters, the LODs were 11 nM and 9.0 nM for AC and HQ, respectively. The linear ranges were 0.2 μM to 0.1 mM for AC and 0.1 μM to 0.1 mM for HQ, as also categorized in Table 2. Anti-interference studies showed that 10-fold amounts of AA, UA, DA, and 20-fold of inorganic ions had no effect on the determination of 10 μM AC and HQ, indicating a moderate selectivity of the method. This work was beneficial for the electrochemical determination of both HQ and AC from whitening cream and pill samples (dissolved in pH 6 PBS) with recovery percentages of 95.2% to 96.0% for AC and 94.5% to 96.2% for HQ.

Jin and coworkers[72] modified an indium tin oxide (ITO) sensor with a hybrid nanozyme material Nafion/GO-AuNP to develop an electrochemical sensor to detect H_2O_2 using 3,3,5,5,-tetramethylbenzidine (TMB) as a redox mediator. The GO-AuNPs hybrid nanomaterial was synthesized by adding to a GO dispersion a gold precursor, $HAuCl_4$, and sodium citrate. The obtained nanozyme material was drop cast added on ITO substrate and incubated for 12 h at 4 °C, followed by dropping 5 μL of 2% Nafion to get the Nafion-GO-AuNPs/ITO sensor. The linear current response achieved with the modified ITO electrode was in the concentration range of 10 nM to 10 mM with a LOD of 1.9 nM. The stability studies of the electrodes were performed at 4 °C for a week, and the current response for H_2O_2 displayed a deviation with an RSD of 7.8%. No selectivity studies or real sample analyses were performed (Fig. 4).

Sialic acid (SA), chemically called *N*-acetylneuraminic acid, is a key constituent of glycoprotein on the eukaryotic cell membrane and has become a wide and efficient tumor marker. SA played a notable role in the early diagnosis of the malignant conversion of cells because the amount of SA is strongly linked to the metastasis, tumor antigenicity, infiltration, and proliferation of therioma.[87]

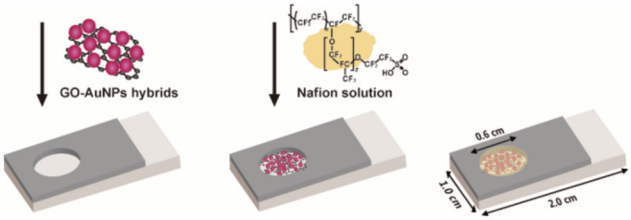

Fig. 4 Structure of the Nafion/GO-AuNP hybrid modified ITO electrode (reprinted from ref. 72 with permission granted from Elsevier).

An extremely selective SA nanozyme-based electrochemical sensor was reported[76] for the first time using an indicator displacement assay (IDA) of DA. IDA is a new approach for electrochemical detection, and it is a competitive response mode between the indicator and the analyte.[88] The main benefit of IDA is that the indicator does not need to covalently integrate the molecular recognition component, so it is likely to choose a receptor or indicator.

For this study, the authors selected dopamine (DA) as an indicator to achieve the detection of SA by IDA. The sensor was designed using a composite material of tetra(4-carboxyphenyl) porphyrin (TCPP)-GO, DA, and 2-fluorophenylboronic acid (FPBA). The GO and TCPP were dispersed by sonication, and 5 μL from the obtained composite was cast on top of a GCE (3 mm diameter). The TCPP-DA/GCE was immersed for several minutes into a solution formed by the complex NHS/EDC and left to dry in the air. In the subsequent step, 5 μL of 10 mM DA were added to the surface of the sensor and left to interact, and then reacted also with FPBS solution to finish the final modification step, and the functionalized GCE was constructed. The linear concentration range was between 0.1 and 7.5 μM, with LOD 28.5 μM. The amino acids valine, cysteine, and tryptophan were investigated as interfering species, and they showed almost no alteration in signal for detection of SA, whereas the structural analogs AA, UA, and glucose showed notable interferences. For this reason, in the pre-treatment step of the samples, an ion-exchange extraction was performed to purify the biological samples in order to increase the selectivity of the method. Pretreated urine and blood samples were tested using the developed sensor, and the results showed recovery from 97% to 104%, proving the practicability of the sensor.

State-of-the-art coordination polymers (CPs) based on hybrid metal (*e.g.*, Ag) and thiol complexes have fascinating physical properties and have been used in versatile applications.[89,90] It is recognized that the thiol-Ag(I) CP is designed by the reaction of thiol with Ag(I). As a rule, amino acids can chelate with Me atoms through their amino-N and carboxylate O_2. Due to its ease of preparation procedure and exciting chain-like structure with various functional groups, thiol-Ag(I) CP shows promise for applications in biosensing.[91,92]

Graphene functionalization with a protein-mimicking nanowire (PMN) based on L-cysteine-Ag(I) coordination polymer was reported by Zhang *et al.*,[71] in 2018, for sensing H_2O_2 from human serum and urine. The PMN was synthesized

from $AgNO_3$ and L-Cys in double-distilled water by incubation and stirring to obtain the L-Cys-Ag(I)CP. The design of the biosensor was based on the electrochemical deposition of GO on top of the GCE by the CV technique and −1.5 to 0.5 V, followed by 8 μL of L-Cys-Ag(I)CP and 0.5% Nafion coated on top of the GO/GCE. For storage, the biosensor was kept in the fridge. The L-Cys-Ag(I)CP-GO/GCE showed low charge transfer resistance, high current intensity, and a smaller peak-to-peak separation than GO/GCE and bare GCE (Fig. 5(A) and (B)) when it was characterized using the redox couple $[Fe(CN)_6]^{3-/4-}$. The reduction of H_2O_2 occurred at −0.8 V (Fig. 5(C and D)), and the linear concentration range was from 0.001 to 5.0 mM with a LOD of 0.3 μM. The coexisting compounds, DA, AP, UA, citric acid (CA), K^+, Ca^{2+}, and GLU, showed no interference in the determination of H_2O_2. The feasibility of L-Cys-Ag(I)CP-GO/GCE was investigated using bio samples, and the recovery percentage ranges were 98.3–103% for serum samples and 98.8–101% for urine samples.

Aminated polyamidopamine dendrimers (PAMAM) have drawn much consideration due to their vastly branched and 3D macromolecules with numerous amine groups at the edges.[93] The functional groups of the PAMAM dendrimers can gather numerous metal ions, becoming an excellent sensing material in biosensing applications.

A 2D composite was prepared from GO and PAMAM through covalent interaction and reported as a carrier for iron

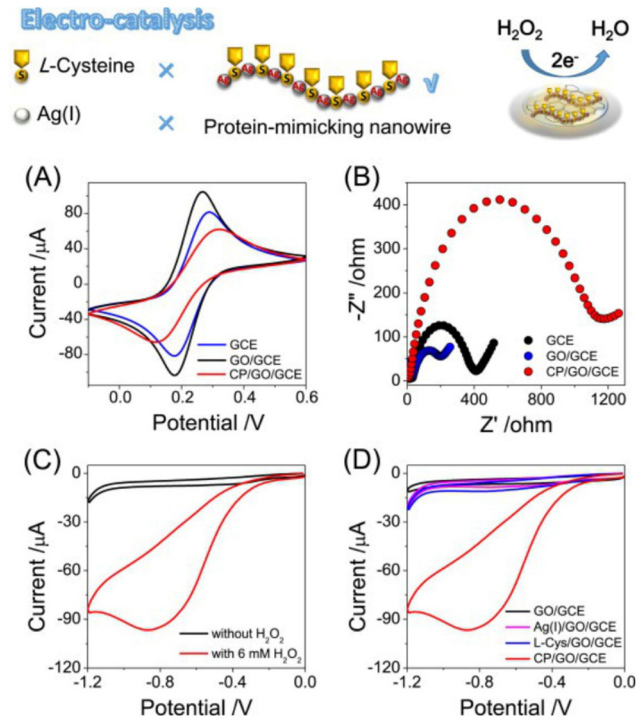

Fig. 5 (A) Cyclic voltammogram and (B) EIS of the bare GCE, GO/GCE and CP/GO/GCE in 5 mM $[Fe(CN)_6]^{3-/4-}$ containing 0.1 M KCl; (C) cyclic voltammograms of CP/GO/GCE in the presence or absence of 6 mM H_2O_2; (D) cyclic voltammograms of GCE, Ag(I)/GO/GCE, L-Cys/GO/GCE and CP/GO/GCE in 0.1 M PBS (pH 7.0) containing 6 mM H_2O_2 (reprinted from ref. 71 with permission from Elsevier).

(II) ions, forming the PAMAM–GO–Fe^{2+}-modified GCE for the detection of H_2O_2 from milk samples.[70] The PAMAM–GO–Fe^{2+} was prepared as follows: the complex of NHS/EDC was added to the dispersed GO and left to react for several minutes to provide GO with active carboxylic groups. An amount of PAMAM dendrimer was drop-cast onto the GO suspension and left for 12 h at room temperature to react. After that, $FeCl_2$ was added to the GO-PAMAM suspension and stirred overnight until PAMAM assembled multiple iron ions. The as-formed PAMAM–GO–Fe^{2+} was cast on top of GCE and dried under an air atmosphere. For further use, the proposed electrochemical sensor was stored in the fridge, and tested for 3-week stability. The increase of peak current was proportional to the H_2O_2 concentration in a range from 500 nM to 2 mM. The sensitivity was 2.71 μA μM^{-1} cm^{-2}, and the LOD was 180 nM based on the $3\sigma/S$ methods. The coexisting species AA, UA, DA, and glucose were investigated, and no interference was observed in the detection of H_2O_2 at the PAMAM–GO–Fe^{2+}/GCE. H_2O_2 acts as a preservative and is often added illegally to milk; thus, spiked buffered milk samples were explored to assess method feasibility, and the recoveries were found to vary from 93.0 to 100.8%. Pre-treated disinfected fetal bovine serum samples were buffered and spiked with H_2O_2, and the average recovery rate was 97%. These results highlighted the good accuracy of the proposed sensor.

Among the reported porous materials, metal–organic frameworks (MOFs) are a novel division of porous crystalline materials, composed of hybrid organic–inorganic supramolecular materials with a high surface area, porous with specified pore sizes. With properties such as long-lasting porosity, high surface area, and catalytic activity, along with thermal and chemical stability,[94] MOFs are excellent materials for electrode modification.

In 2019, Soltani-Shahrivar and coworkers[77] used a 35MIL-101(Fe)-rGO nanocomposite to modify the surface of a GCE for the determination of two carbamate insecticides, carbofuran (CBF) and carbaryl (CBR). The carbamate insecticides are categorized as hazardous constituents that copy the mechanism of organophosphate pesticides but have a smaller action period,[95] and they can enter the human body through contaminated food, water, or air. The synthesis of the materials used in the design of the sensor was laborious and is just briefly described here. The GO powder, $Fe(NO_3)_2{\cdot}3H_2O$ and H_2BDC, were dispersed in DMF separately, and then Fe $(NO_3)_2{\cdot}3H_2O$ was added to the GO suspension and sonicated. After 15 minutes, H_2BDC was also added and the sample was sonicated again for 15 minutes. The solvothermal method continued with thermal treatment of the final mixture and a drying procedure, and 35MIL(Fe)-101@GO and 35MIL(Fe)-53@GO were obtained. Both were dispersed in EtOH, and a few μL were dispersed on two GCEs to form the 35MIL(Fe)-101@GO/GCE and 35MIL(Fe)-53@GO/GCE, and the calculated active areas were 0.262 cm^2 and 0.173 cm^2, respectively. The higher surface area of 35MIL(Fe)-101@GO/GCE is due to the higher pore volume. Due to better electrochemical performances, the 35MIL(Fe)-101@GO/GCE material was further inves-

tigated for CBF and CBR, and under optimal conditions the LODs were 1.2 and 0.5 nM within the linear ranges of 5.0–200.0 nM and 1.0–300.0 nM for CBF and CBR, respectively, as also shown in Table 2. A 200-fold excess of Co^{2+}, Ni^{2+}, Cu^{2+}, Cd^{2+}, K^{+}, Ca^{2+}, Mg^{2+}, Fe^{3+}, Al^{3+}, Ni^{2+}, Zn^{2+}, Cu^{2+}, F^{-}, Cl^{-}, Br^{-}, SO_4^{2-}, PO_4^{3-}, NO_3^{-} and CO_3^{2-} and also the presence of diazinon, malathion, paraoxon, parathion, and fenamiphos had an error of less than 5%, and so have no influence on the signals of CBF and CBR. Several fruits and vegetables (cucumber, oranges, tomatoes, and cabbage) were used to prove the applicability of 35MIL(Fe)-101@GO/GCE for the simultaneous detection of CBF and CBR, and the results showed recovery percentages between 98.0% and 104.7%.

Metal molybdate compounds, $MeMoO_4$, have lately played an important role as electrocatalytic materials in the electrochemistry field.[96,97] Due to this electrocatalytic behavior, in 2020,[79] a $NiMoO_4$ was used to functionalize GO for the modification of a screen-printed carbon electrode (SPCE) for the determination of CAT from industrial, domestic, and underground waters. The GO material overcomes the poor electrochemical stability of the $NiMoO_4$, which happens because of structural breakdown during redox reactions. The $NiMoO_4$ material (Fig. 6B) was synthesized using the hydrothermal method, using nickel nitrate hexahydrate, urea, and ammonium molybdate tetrahydrate as precursors. After the precipitate was washed and dried, it was mixed with GO (Fig. 6A) and distilled water and ultrasonicated to obtain the nanocomposite denoted $NiMoO_4$@GO (Fig. 6C and D). The LSV results were recorded in a very wide linear range of 0.01–273.0 μM, the LOD was calculated to be 1.59 nM, as tabulated in Table 2, and the sensitivity of the sensor was 46.4 μA μM^{-1} cm^{-2}. The sensor exhibited a stable current response for CAT in the presence of potentially interfering species such as HQ, DA, AA, EP, UA, and glucose and 200-fold addition of common ions such as Na^{+}, K^{+}, Mg^{2+}, Cl^{-}, HPO_4^{2-}. The $NiMoO_4$@GO/SPCE exhibited a good response towards the detection of CAT from real complex samples, having values in the range of 99.0–101.5% for recovery studies.

A nonenzymatic urea sensor based on the nickel sulfide (NiS)/GO-modified GCE was reported,[80] in 2020. The NiS is a transition metal compound that displays a strong inclination to form complex coordination. Sulphide (S^{2-}) can donate e^{-} to Ni atoms, which causes higher electron density on nickel. NiS is also used as an active catalyst due to its electronic interaction activity and abundant redox reactions, but it has poor stability during electrochemical reaction;[99] that is why GO is employed as material in the design of the proposed urea sensor. The morphology and XRD spectra of the NiS/GO are presented in Fig. 7. The NiS/GO was prepared using the hydrothermal method, starting from a mixture of GO dispersion, $NiCl_2$, and L-Cys, that was stirred and then subjected to thermal treatment for 24 h. Finally, the compound was dried under a vacuum and then redispersed in DMF. A few μL of NiS/GO were drop-cast on top of a GCE, and the sensors were evaluated for the detection of urea. The NiS/GO/GCE was further evaluated for the detection of urea, and the response was linear in a concentration range of 0.1–1.0 mM, with a LOD value of 3.79 μM. Glucose, UA, and AA were tested for interference in the determination of urea using the proposed sensor, and no change or only a slight change in response was recorded. The method was applied for measuring urea from milk samples with a percentage of recovery in the range of 98.6–99.4%.

In 2021, Liu, Zhang, and Zheng[73] proposed an AuNPs-PB-GO nanomaterial for the electrochemical detection of H_2O_2. The hybrid material was prepared through a facile one-pot strategy as follows: the GO powder was first obtained by the Hummers method and dispersed in water, then $FeSO_4$ and $K_4[Fe(CN)_6]$ were successively added to the flask containing the

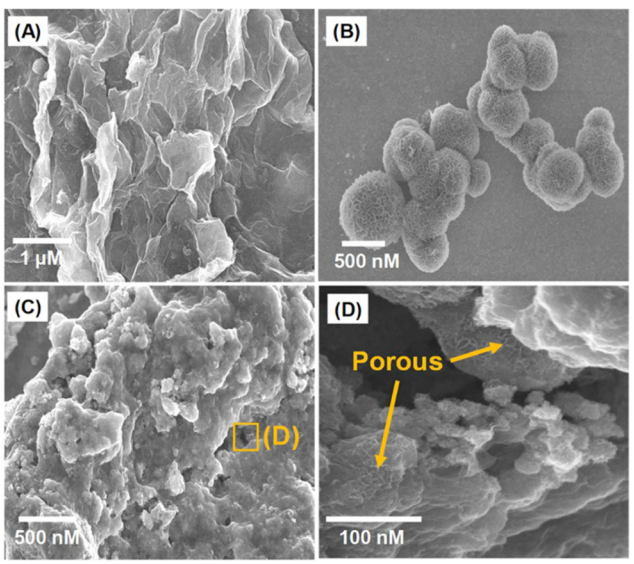

Fig. 6 The FE-SEM images of GO (A), $NiMoO_4$ (B), $NiMoO_4$@GO (C), and the higher magnification of $NiMoO_4$@GO (D) (reprinted from ref. 79 with permission from Elsevier).

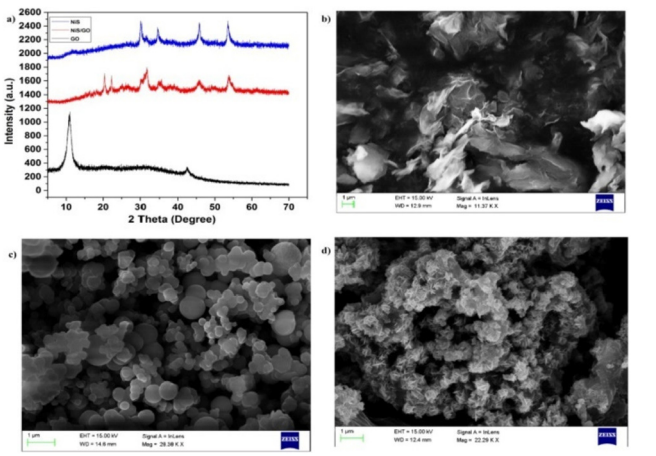

Fig. 7 (a) XRD pattern obtained for GO, NiS, and NiS/GO, (b) SEM image recorded for GO, NiS (c), and NiS/GO (d) (reprinted from ref. 80 with permission from Elsevier).

dispersed GO solution, and stirred for 10 minutes. Following this, a few mL of $HAuCl_4$ aqueous solution was dropped into the system which was stirred for 24 h; afterward it was centrifuged and collected. A small amount of the final product, AuNPs-PB-GO, was dispersed in water, and 10 μL were drop-cast on top of a GCE that was modified with 5% Nafion solution and was left to dry under an air atmosphere. The prepared AuNPs-PB-GO/GCE was electrochemically studied for H_2O_2 detection, proving to have nanozyme features. The current response of the sensor towards the reduction of H_2O_2 was linear for a concentration range from 3.8 to 5400 μM with a detection limit of 1.3 μM as shown in Table 2, and a sensitivity of 87.6 μA mM^{-1} cm^{-2}. In the presence of possible interfering species, such as glucose, AA, uric acid (UA), and acetaminophen (AP), the signal of H_2O_2 recorded at the AuNPs-PB-GO/GCE showed no changes in current intensity, proving a selective response towards H_2O_2. The developed sensor showed favorable repeatability, stability, and reproducibility results, but no real samples were analyzed to test the applicability of the method.

Reduced GO (rGO) composites as nanozymes for electrochemical sensing

Nanozyme materials benefiting from all the advantages of rGO nanomaterial have also been intensively studied for the determination of inorganic compounds such as H_2O_2,[100–107] nitrite,[108,109] organic compounds, CAT,[110–114] HQ,[110,112,114,115] chicoric acid,[116] xanthine,[117] methyl parathion and 4-nitrophenol,[118] and also biomolecules such as hormones,[119,120] cancer biomarkers,[121–124] AA,[125,126] and glucose,[127] as summarized in Table 3.

A PANi–Fe_2O_3–rGO composite was proposed by Radhakrishnan *et al.*[115] for the determination of HQ from tap water, and its characteristics are summarized in Table 3. The Fe_2O_3-rGO composite was prepared by a hydrothermal method by dispersing GO in ethanol, followed by the addition of $FeCl_3$ and 25% ammonia. The PANi–Fe_2O_3–rGO composite was prepared by *in situ* polymerization of aniline monomer in the suspension of Fe_2O_3–rGO, and the composite ratio with better electrochemical performances was 5 : 1 (Fe_2O_3-rGO to aniline). The interconnection between the PANI nanofibers and Fe_2O_3–rGO sheets proved to increase the electrocatalytic activity of the HQ sensor. A volume of 10 μl from the prepared composite was cast above the GCE and allowed to dry at room temperature. For further analytical investigations, the authors proposed pH 2.5 as the optimum pH to reduce the chances of deprotonation of HQ once the pH becomes more alkaline. For the concentration range from 0.1 to 550 μM, PANi–Fe_2O_3–rGO/GCE showed a linear response, with a LOD of 0.06 μM. The anti-interference ability of the PANi–Fe_2O_3–rGO composite was tested for the detection of HQ from mixed solutions containing various common ions such as Cl^-, Zn^{2+} Mg^{2+}, Ca^{2+}, Na^+ and Cu^{2+} and some physiological interferents such as glucose, urea, and ethanol. Only a slight change in the DPV current response was observed for 25 μM HQ. The selectivity was also tested in the company of 100-fold additional CAT, and the response remained the same for HQ determination. The recovery percentages from tap water samples were between 97.3 and 101.6%.

In 2016, a nanozyme electrochemical sensor based on PtNPs/rGO-chitosan-ferrocene carboxylic acid nano-hybrids (PtNPs/RGO-CS-Fc)[100] was developed for the measurement of H_2O_2 in order to evaluate oxidative stress in living cells. The rGO-CS-Fc nanohybrid material was prepared by mixing CS (acetic acid 1%) with ferrocene acid, EDC, and sulfo-NHS solution, and stirred for 4 h. rGO dispersed in water was added to the system when the color of the mixture turned from yellow to reddish-brown, and stirred for 24 h. A small volume of the nanomaterial was dropped on top of a cleaned gold electrode (AuE) and incubated for 30 min at 37 °C. After this, the PtNPs were electrodeposited on top by chronoamperometry at −0.2 V, under mild stirring, using $PtCl_6$ as the precursor, and the final sensor was obtained and denoted PtNPs/RGO-CS-Fc/AuE. The design of the sensor is illustrated and presented in Fig. 8. The prepared sensor was stored in humid conditions, in the fridge, prior to use, and after 22 days, 80% of its initial current response was recorded. The current response of the biosensor presented a linear relationship with H_2O_2 concentration from 20 nM to 3 μM, as tabulated in Table 3, with a correlation coefficient of R^2 = 0.9968 and with a LOD value of 20 nM. The response of the PtNPs/RGO-CS-Fc/AuE towards H_2O_2 was investigated in the presence of glucose, UA, and AA, and it was not changed, showing no interference from coexisting species.

An interesting approach to proving the ability of the developed sensor, by testing cell lines, was selected by the authors. A similar recorded current of H_2O_2 was released by the same precise quantity of A549, HepG2, and L02 cell lines when stimulated by 1 μM AA. The tumor cells (A549, HepG2) produced more H_2O_2 than normal cell lines (L02), which showed that irregular growth of the tumor enhanced ROS production capacity, and this is relevant for further cancer therapy-related investigations.

CdS nanoparticles, as a class of t-metal dichalcogenides, are of great interest in developing biosensors.[134] Hu and coworkers[114] described the modification of GO surface with CdS, obtaining the CdS-rGO nanomaterial employed for the determination of dihydroxybenzene isomers. The GO classical synthesis method was followed by another two steps for the final synthesis of CdS-rGO. GO was dispersed in water, and $(CH_3COO)_2Cd$ was formed from $CdCO_3$ and EtOH. $(CH_3COO)_2Cd$ and GO were dispersed by ultrasonication in 30 mL DMSO for 20 min. Afterward, a hydrothermal process that caused the reduction of GO, the brownish-green CdS-rGO product, was obtained. After cleansing with alumina powder, the GCE was functionalized by drop-casting 6 μL of CdS-rGO on top and left to dry at room temperature. The linear concentration ranges for CAT, HQ, and RC were 0.5 to 1350 μM, 0.2 to 2300 μM, 1.0 to 500 μM, respectively. LLODs were calculated for CAT, HQ, and RC to be very low at 0.054 μM, 0.09 μM, and 0.23 μM, respectively, reported for a signal-to-noise ratio of 3. Some possible interfering species in the concurrent detection of CAT, HQ, and RC were examined, such as 150-fold K_2SO_4,

Table 3 Some selected reduced graphene oxide composites as nanozymes for electrochemical sensing

Nanozymes	Substrate	Method	Transducer	Medium	Linear range	LOD	Application	Ref.
rGO/CS/Fc	H_2O_2	AMP	Pt	0.02 M PBS (pH 7.0)	0.02–3 μM and 6–10 000 μM	0.02 μM	Living cells	100
3D MoS_2/rGO	H_2O_2	AMP	GCE	0.01 M PBS (pH 7.4)	2–23 180 μM	0.19 μM	Human serum	101
CuNPs-rGO	H_2O_2	CA	GCE	0.1 M PBS (pH 6.5)	100–18 000 μM	0.6 μM	Lens-cleaning solution	102
$NiCo_2O_4$/$CoNiO_2$@pRGO	H_2O_2	AMP	GCE	0.1 M PBS (pH 7.4)	5–3000 μM and 3000–12 000 μM	0.41 μM	Living cancer cells	103
rGO/PANI@Pt rGO/PANI@PtNi	H_2O_2	AMP	GCE	0.2 M PBS (pH 6.5)	100–126 400 μM	1.1 μM 0.5 μM	NS	104
rGO-PT-Pt NPs	H_2O_2	AMP	SPCE	PBS (pH 7.4)	1–100 μM	0.26 μM	Human serum	105
Ag/boehmite NTs/rGO	H_2O_2	AMP	GCE	0.1 M PBS (pH 7.2)	0.5–10 000 μM	0.17 μM	Disinfectant sample	106
$La_{0.6}Sr_{0.4}CoO_{3-\delta}$/rGO	H_2O_2	AMP	GCE	0.1 M NaOH	0.2–3350 μM	0.05 μM	NS	107
rGO–MOS_2–PEDOT	Nitrite	DPV	GCE	0.1 M PBS (pH 4.0)	1–1000 μM	0.059 μM	Tap water, pond water, packaged drinking water and milk	108
His@AuNCs/rGO	Nitrite	DPV	GCE	0.1 M PBS (pH 7.0)	1–7000 μM	0.5 μM	Sausage	109
CDs/rGO	HQ CAT	DPV	GCE	PBS (pH 7.0)	0.5–1000 μM 1.0–950 μM	0.17 μM 0.28 μM	Tap, river water and industrial sewage	110
Au-PdNFs/rGO	HQ CAT	DPV	GCE	0.1 M PBS (pH 7.0)	1.6–100 μM 2.5–100 μM	0.5 μM 0.8 μM	Tap, lake and river water	112
Au/$Ni(OH)_2$/rGO	CAT	DPV	GCE	0.1 M PBS (pH 6.0)	0.4–33.8 μM	0.13 μM	Lake water	113
CdS/rGO	HQ CAT	DPV	GCE	0.1 M PBS (pH 7.0)	0.2–2300 μM 0.5–1350 μM	0.054 μM 0.09 μM	Tap, well and river water	114
PANi–Fe_2O_3–rGO	HQ	DPV	GCE	PBS (pH 2.5)	0.1–550 μM	0.06 μM	Tap water	115
Au@Pt-PEI-rGO	Chicoric acid	DPV	GCE	Na_2HPO_4–citric acid solution (pH 3.0)	0.3–30 μM	0.0048 μM	NS	116
CuS@Pd/N-rGO	Xanthine	DPV	GCE	0.1 M PBS (pH 3.7)	0.7–200 μM	0.028 μM	Chicken serum and human urine	117
NiS_2-rGO/curcumin NPs	Methyl parathion	DPV	GCE	0.1 M PBS (pH 7.4)	0.25–80 μM	0.0087 μM	Tomato, apple juices and river water	118
$NiCo_2O_4$/$CoNiO_2$@pRGO	4-Nitrophenol	AMP	GCE	0.1 M PBS (pH 7.4)	5–3000 μM and 3000–12 000 μM	0.0069 μM	Living cancer cells	103
Pd/N-rGO	Estradiol	DPV	GCE	PBS (pH 7.0)	0.1–400 μM	0.0018 nM	Human urine and milk,	119
Co_3O_4–CuNi–rGO	Ascorbic acid	AMP	GCE	0.1 M PBS (pH 7.0)	2.5–100 μM	0.34 μM	vitamin C tablets, orange, and vitamin water	126
$Ni(OH)_2$-PEDOT-rGO	Glucose	AMP	GCE	0.1 M NaOH	2–7100 μM	0.6 μM	Human serum	127
GO-MF	CAT	DPAV	GCE	0.1 M PBS (pH 7.0)	0.01–0.1 μM	0.00051 μM	NS	128
Ag-Fe_2O_3/POM/rGO	H_2O_2	AMP	GCE	0.1 M PBS (pH 6.8)	0.3–3 × 10^3 μM	0.2 μM	Environmental water samples	129
Aptamer/AuPd NPs@ rGO/MWCNTs	Oxaliplatin	DPV	GCE	PBS (pH 7.0)	0.00018–0.170 μM	0.00006 μM	Pharmaceutical injection, human serum, human urine	130
Cu nanocubes/rGO	Dopamine	DPV	SPCE	BRB (pH 6.0)	0.001–100 μM	0.00033 μM	Human plasma samples	131
CoO/N–carbon sheet/rGO	Dopamine uric acid	DPV	GCE	PBS (pH 7.0)	0.5–110 μM 1.0–125 μM	0.15 μM, 0.22 μM	Human serum	132
Co–N–C rGO aerogel	H_2O_2, dopamine and uric acid	AMP	GCE	PBS (pH 7.0)	3.00–2991 μM	0.74 μM	Human urine	133
Au@Pt-PEI-rGO	Chicoric acid	DPV	GCE	Na_2HPO_4–citric acid solution (pH 3.0)	0.3–30 μM	0.0048 μM	NS	116
CuS@Pd/N-rGO	Xanthine	DPV	GCE	0.1 M PBS (pH 3.7)	0.7–200 μM	0.028 μM	Chicken serum and human urine	117
NiS_2-rGO/curcumin NPs	Methyl parathion	DPV	GCE	0.1 M PBS (pH 7.4)	0.25–80 μM	0.0087 μM	Tomato, apple juices and river water	118
CdS/rGO	4-Nitrophenol	DPV	GCE	0.1 M PBS (pH 7.0)	0.2–2300 μM	0.0069 μM	Tap, well and river water	114
Pd/N-rGO	Estradiol	DPV	GCE	PBS (pH 7.0)	0.1–400 μM	0.0018 nM	Human urine and milk	119
Co_3O_4–CuNi–rGO	Ascorbic acid	AMP	GCE	0.1 M PBS (pH 7.0)	2.5–100 μM	0.34 μM	Vitamin C tablets, orange, and vitamin water	126

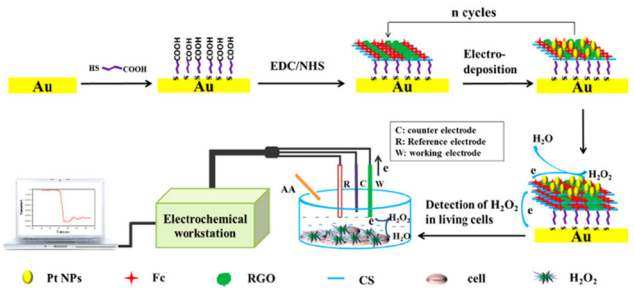

Fig. 8 Analytical principle for the detection of H_2O_2 in living cells with the nonenzymatic biosensor based on PtNPs/RGO-CS-Fc nanohybrids (reprinted from ref. 100 with permission from Elsevier).

$MgCl_2$, and NaCl, and 100-fold of Ph, NP, and GLU with no change in the current response, showing a good selectivity of the sensor. Real water samples were spiked with two different concentrations of all three dihydroxybenzene isomers and were investigated using the CdS-rGO/GCE. The results of the spiked samples were between 96.8% and 102.7% recovery, proving a good applicability of the proposed method.

Multifarene[*m*,*n*] (MF[*m*,*n*]) were reported, in 2014, by Parvari and coworkers[98] as new modular cavitands, being constructed of alternating building blocks which consisted of *m* 4-*t*-butylphenol units and *n* 2-imidazolidinone or 2-imidazolidinetione units linked by methylene bridges. In 2020, Luo and coworkers[128] designed an rGO-MF based-electrode for the sensitive determination of CAT and DA. The preparation procedure for MF was taken from the literature,[98] and further, the MF was dissolved in DMSO and mixed with rGO (also dispersed in DMSO). The mixture was stirred for 24 h to obtain the rGO-MF suspension material, which was drop-cast on top of the GCE. The quantitative analysis of CAT was obtained with rGO-MF/GCE in the linear concentration ranges of 10 nM–100 nM and 0.1–100 μM, having a LOD value of 0.51 nM. Furthermore, the developed method was able to detect DA, a derivative of CAT, in the linear concentration ranges of 10–100 nM and 5–100 μM with LOD 0.62 nM. There were reported insignificant effects of 200-fold of GLU, 30-fold urea, and 20-fold AA for the detection of DA. The sensor was also tested in DA injection samples and obtained a recovery range between 99% and 113%.

In 2021, rGO functionalized with molybdenum disulfide (MoS_2) with a lattice spacing of 0.62 nm was reported[101] for the MoS_2–rGO design of a nanozyme-based H_2O_2 sensor. The MoS_2/rGO nanozyme was synthesized by a one-pot hydrothermal method, using GO and Na_2MoO_4 as precursors for rGO and MoS_2, respectively. The nanocomposite was dispersed in 0.05 CS solution (acetic acid) and sonicated. A volume of 5 μL from the obtained uniform dispersion was drop-cast on top of a GCE to form the MoS_2–rGO/GCE. The nanozyme sensor composed of this electrode has a good linear dependence on the H_2O_2 concentration in the range of 2 μM to 23.18 mM, and the LOD was 0.19 μM. The following potential interference substances were selected for selectivity studies: DA, UA, AA, glucose, serine, alanine, Na^+, K^+, Mg^{2+}; no change in the recorded chronoamperograms was observed when a 5-fold concentration of the above substances was added to the H_2O_2 solution. The MoS_2–rGO/GCE was evaluated for analytical applications in serum samples, and the recovery range was 97%–108%.

In 2021, Gugoasa, Kurbanoglu, and collaborators[111] developed a nanozyme-based sensor using Gr decorated with AuNPs nanohybrid material for the determination of CAT in environmental samples. The nanomaterial was prepared by a simple electrochemical method. The nanohybrid material was drop-cast on an SPE, and its electrocatalytic action for CAT oxidation was compared using a laccase enzyme (Fig. 9). For the nanozyme sensor, the linear voltammetric response was between 1.0 nM to 1.0 mM and showed a high sensitivity (0.048 A/M). The limit of detection was calculated to be 0.33 nM (S/N = 3), while the Michaelis–Menten constant was 1.87 mM for the developed nanozyme sensor and 5 mM for the Lac/SPE, proving better performances of the nanozyme compared with the enzyme. The results displayed negligible current variations in the detection of CAT when 10-fold of Cu^{2+}, 100-fold of HQ, AA, NO^{3-}, 500-fold GLU, K^+, Na^+, Ni^{2+}, Ca^{2+}, Cl^-, Zn^{2+} were tested along with CAT. The proposed sensor was verified for the determination of CAT in real samples, showing very good results of 90.9% to 100.1% recovery of CAT from both mineral and tap water.

A novel electrochemical sensor for the detection of chicoric acid by modifying a GCE with Au@Pt/polyethylenimine (PEI)-rGO nanohybrids was reported.[116] Chicoric acid is a phenolic

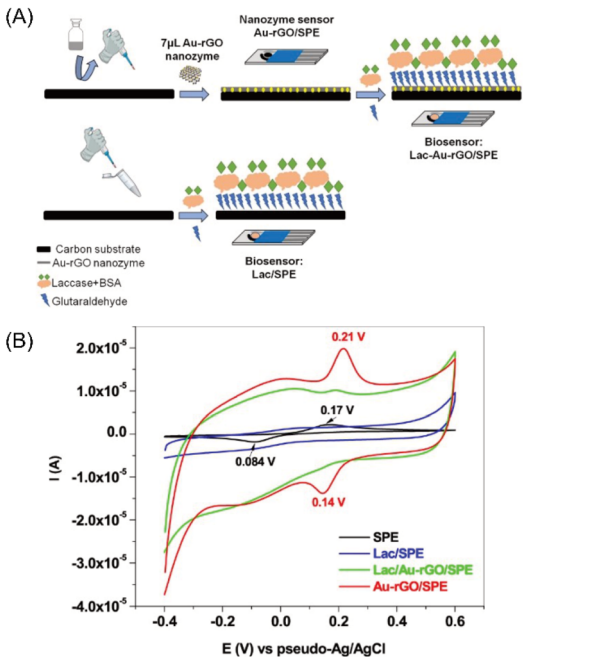

Fig. 9 (a) The schematic design of the nanozyme and biosensors: Au–rGO/SPE, Lac/Au–rGO/SPE, and Lac/SPE; (b) cyclic voltammograms recorded with SPE, Lac/SPE, Lac/AurGO/SPE and Au–rGO/SPE in 0.1 M MII pH 5 containing 10^{-4} M catechol; scan rate 20 mV s^{-1} (reprinted from ref. 111 with permission from IOP Publisher).

compound broadly found in many plants and has drawn extensive attention in the last few years due to its extraordinary anticancer properties. The preparation of PEI-rGO started by adding PEI and KOH to GO, and it was stirred until a homogeneous water dispersion was obtained, followed by a magnetic stirring at 60 °C for 12 h and centrifugation to obtain PEI-rGO. Hexadecyl trimethyl ammonium bromide (CTAB) solution, $HAuCl_4$ as Au precursor, H_2PtCl_6 as Pt precursor, and 0.1 M AA were mixed with the PEI-RGO solution and reacted for 24 h with continuous stirring at room temperature. The obtained suspension of Au@Pt-PEI-rGO was deposited on the GCE by dip-coating. After 30 days, the proposed sensor was stable and retained 95% of the initially recorded signal. The obtained sensor demonstrated efficient chicoric acid detection in the concentration range of 0.3 μM to 0.03 mM, with a sensitivity of 49.357 μA μM^{-1} cm^{-2} and a LOD value of 4.8 nM. No significant current shift was noticed when 25-fold excess of AA, AC, or glucose was added to the system, and the applicability of the method in real samples was not specified.

The synergism of phosphomolybdic acid hydrate decorated with Ag-Fe_2O_3NPs and anchored on rGO was reported to be effective as a nonenzymatic H_2O_2 sensor platform.[129] Polyoxometalates (POMs) are stable and exceptionally negatively charged elements with attractive electronic and chemical versatility. POMs have a solid affinity toward carbon nanomaterials such as graphene due to the opportunity for electron transfer and electrostatic interactions.[135] The POM was deposited following a previously reported method, and it was added to a solution containing rGO in ethylene glycol to obtain the POM-rGO product. $AgNO_3$ (as Ag precursor) and Fe $(NO_3)_3$ (as Fe precursor) were mixed with POM-rGO. Urea and polyethylene glycol (PEG) was added to the system and sonicated for 30 minutes at room temperature. Finally, the $AgFe_2O_3$-POM-rGO nanocomposite was obtained. This material was used to modify the GCE. The developed sensor showed a linear response across the concentration range from 0.3 mM to 3.3 mM (R^2 = 0.992) with a LOD of 0.2 μM and a sensitivity of 271 μA mM^{-1} cm^{-2}. The response current was unaffected after introducing UA, glucose, and EtOH into a solution containing 300 μM H_2O_2. No real sample investigations were performed to attest to the applicability of the sensor.

A hybrid with 3D hierarchical CuS@Pd core–shell cauliflowers decorated on N-doped rGO CuS@Pd/N-rGO was reported[117] for the detection of xanthine, a very important biomarker in the fields of clinical analysis and food quality control. The nanohybrid material was prepared by a facile wet-chemical route without requiring any template molecules and surfactants. First, N-rGO was synthesized by a hydrothermal method from graphite and urea as main precursors. Second, the CuS material was prepared from $CuCl_2$ and thiourea, and after the CuS product was obtained, a few drops of $PdCl_2$ and $NaBH_4$ were sequentially introduced into the system to form CuS@Pd, followed by the addition of N-rGO to the system to obtain the final nanohybrid material: CuS@Pd/N-rGO. The sensor, based on CuS@Pd/N-rGO deposited on GCE, displayed nanozymatic features for the detection of xanthine, including a wide detection range of 0.7–200.0 μM (0.94 V *vs.* SCE), a LOD of 28 nM (S/N = 3), high reproducibility with RSD lower than 4.1%, and commendable stability (retained 90% of the initial signal after 1 month). The presence of 100-fold amounts of UA, glucose, or urea, and 10-fold amounts of AA, DA, guanine, L-Trp, or paracetamol had no significant influence on the DPV signals of xanthine, with an RSD value of less than 5%. Reliable and satisfactory recoveries in a range of 95–105% were achieved for xanthine detection in chicken serum and human urine samples.

Conducting polymers such as polythiophene (PTh), polypyrrole (PPy), poly(3,4-ethylenedioxythiophene) (PEDOT), polyaniline (PANI), and their derivatives have been receiving immense consideration due to their enhanced electrochemical performances.[136] Amongst them, PEDOT has been regarded as one of the most outstanding conducting polymers due to its superior electrocatalytic ability, which has been broadly investigated in electrochemical sensors.[137] Nevertheless, pure PEDOT undergoes an aggregation process during growth, experiencing a diminution of its conductivity which limits its applications.[138] In order to overcome this issue, Madhuvilakk *et al.*[108] proposed a 2D nanocomposite formed from rGO and MoS_2 with PEDOT as sensing nanozyme material for the detection of nitrite in water and milk samples. The rGO–MoS_2 nanocomposite was prepared by using a slightly modified hydrothermal method. A water suspension of rGO–MoS_2 was ultrasonicated with 15 mL EDOT alcoholic solution, and the polymerization process to obtain the rGO–MoS_2–PEDOT was performed in an ice bath, using APS as the initiator. Using the drop-casting technique, 5 μL of the nanocomposite was deposited on a pretreated GCE, to form the WE. A Pt wire and a SCE served as the CE and RE, respectively. DPVs were recorded at different concentrations of nitrite and a linear range was obtained from 0.001 mM to 1.0 mM at the rGO–MoS_2–PEDOT/GCE. Under optimized conditions, the fabricated electrode exhibited good sensitivity (874.19 mA mM^{-1} cm^{-2}), and an LOD value of 59 nM, (S/N = 3). No appreciable change in the corresponding amperometric steady state current density was observed when 100 μM of K^+, Na^+, Zn^{2+}, Cu^{2+}, Mg^{2+}, BrO_3^-, ClO_4^-, CO_3^{2-} and NO_3^- and 200 μM of DA, AA, UA and glucose were added to the solution containing 10 μM nitrite. The results obtained using the rGO–MoS_2–PEDOT/GCE for detection of nitrite in tap water, pond water and packaged drinking water samples were 99–100.56%, 97.3–99.72% and 99.4–102.3%, respectively. This sensor was also tested in milk samples, with recoveries ranging from 98.3 to 100.8%.

The subclass of MOFs zeolitic imidazolate frameworks (ZIFs) integrates the characteristics of MOFs and zeolites. ZIFs offer plentiful active sites, high surface areas, and favorable electronic configuration, and therefore they are good choices as a material for catalysis in energy conversion and sensing.[139] Hierarchical $NiCo_2O_4$–$CoNiO_2$ hybrids embedded in partially reduced graphene oxide (pRGO) were reported[103] as nanozymes for the design of an H_2O_2 sensor. The 3D structure of pRGO can efficiently limit the aggregation of the fixed NPs, achieving decent stability of the nanohybrid. The CoNi-

ZIF@pRGO nanohybrid was prepared *via* an ion-assistant solvothermal method, starting from $Co(NO_3)_2{\cdot}6H_2O$ (0.55 g) and $Ni(NO_3)_2{\cdot}6H_2O$ as precursors. As for the $NiCo_2O_4$/$CoNiO_2$@pRGO nanohybrid preparation, the black CoNi-ZIF@pRGO powder was separately annealed in a tube furnace. Three temperatures (300 °C, 600 °C, 900 °C) were tested, and at 600 °C the best results were obtained, and for this reason, it was further used to modify the surface of a GCE by the drop-casting technique to obtain the $NiCo_2O_4$/$CoNiO_2$@pRGO/GCE (Fig. 10). This sensor presented two linear ranges obtained in H_2O_2 concentration ranges of 5 μM to 3 mM and 3 mM to 12 nM, with a LOD value of 0.41 μM and two declared sensitivities of 1.295 μA μM^{-1} cm^{-1} and 0.936 μA μM^{-1} cm^{-1}, respectively.

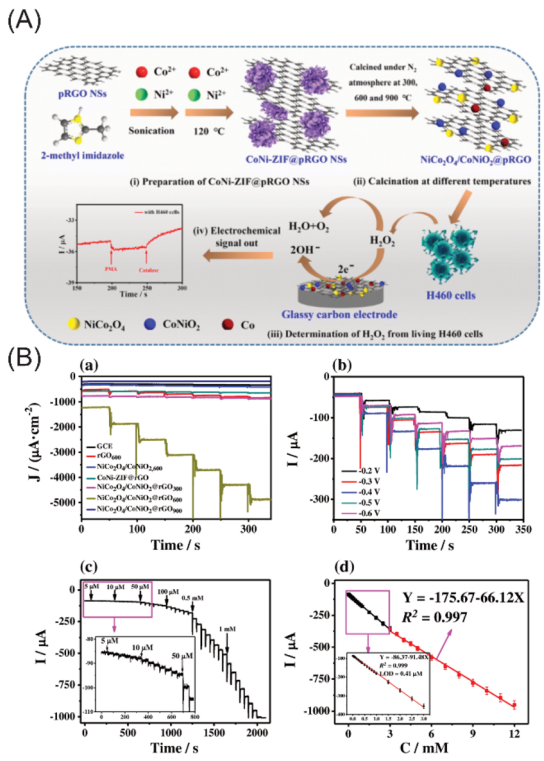

Fig. 10 (A) Synthesis of $NiCo_2O_4$/$CoNiO_2$@pRGO for real-time monitoring of H_2O_2 released from living cancer cells, including (i) preparation of CoNi-ZIF@pRGO NSs, (ii) calcination of CoNi-ZIF@pRGO NSs at different temperatures, (iii) determination of H_2O_2 from living cancer cells, and (iv) electrochemical signal out. (B) (a) Amperometric response of the bare GCE, $pRGO_{600}$, $NiCo_2O_4$/$CoNiO_{2\text{-}600}$, CoNi-ZIF@pRGO, $NiCo_2O_4$/$CoNiO_2$@$pRGO_{300}$, $NiCo_2O_4$/$CoNiO_2$@$pRGO_{600}$, and $NiCo_2O_4$/$CoNiO_2$@$pRGO_{900}$-modified GCEs by stepwise addition of H_2O_2 (concentration range from 500 to 3000 μM) into the N_2-saturated phosphate buffer at an applied potential of −0.4 V *vs.* Ag/AgCl. (b) Amperometric response of $NiCo_2O_4$/$CoNiO_2$@$pRGO_{600}$ modified GCEs by stepwise addition of H_2O_2 (concentration 500, 1000, 1500, 2000, 2500, and 3000 μM) into the N_2-saturated phosphate buffer at different potential (−0.2, −0.3, −0.4, −0.5, and −0.6 V *vs.* Ag/AgCl). (c) Amperometric response of $NiCo_2O_4$/$CoNiO_2$@$pRGO_{600}$/GCE by stepwise addition of H_2O_2 (concentration range: from 5 μM to 12 mM) into the N_2-saturated phosphate buffer at an applied potential of −0.4 V *vs.* Ag/AgCl. (d) Calibration plots of current response *vs.* H_2O_2 concentration from 5 μM to 12 mM at potential of −0.4 V *vs.* Ag/AgCl (reprinted material from ref. 103, Springer-Verlag GnbH Austria, part of Springer Nature Publisher).

The sensor was stable over 15 days when kept at 4 °C. When measuring the H_2O_2 solution in the presence of AA, UA, DA, glucose, and NaCl, the current response was just slightly changed at the $NiCo_2O_4$/$CoNiO_2$@pRGO/GCE. The applicability was tested on living H460 cells, and the results confirmed that the nanohybrid can accumulate the cell with good affinity and targetability to determine the amount of H_2O_2 released from the living cells. Also, the nanohybrid was tested and showed very good biocompatibility.

Liu and collaborators[109] demonstrated that histidine-capped Au nanoclusters (His@AuNCs) possessed intrinsic oxidase-like activity and proposed this nanozyme material for the detection of nitrite in sausage samples. The His@AuNCs were prepared in an ultra-facile one-step blending manner, starting from histidine and $HAuCl_4$ as Au precursor, and kept in the fridge prior to use. The GO and rGO were synthesized by the classical Hummers method. The nanozyme biosensor His@AuNCs-rGO/GCE was employed for the electrochemical determination of nitrite within the linear range 2.5–5700 μM. Using the DPV method, the sensitivity and the LOD of nitrite on His@AuNCs/rGO–GCE were calculated to be 1.07 μA μM^{-1} cm^{-2} and 0.7 μM, respectively. Using the CA method at a constant potential of 0.8 V, the linear range and the LOD of nitrite were calculated to be 1.0–5700 μM and 0.5 μM, respectively.

When 20-fold of NO_3^-, Cl^-, CO_3^{2-}, SO_4^{2-}, Br^-, HCO_3^-, PO_4^{2-}, and AC^- were added to the nitrite solution, no significant modifications in the current intensity were observed. The recovery percentage of nitrite recovered from sausages samples was between 94.6 and 100.2%.

A hierarchical composite based on the modified rGO with Pt–Ni-decorated PANI nanospheres (rGO/PANI@PtNi) was prepared *via* microwave-assisted self-reduction, for the development of a nanozyme-based H_2O_2 sensor.[104] The PANI nanospheres (NS) were synthesized starting from aniline monomer added to a PVA solution and magnetically stirred at room temperature, followed by adding HCl until a brown suspension was obtained, and the addition of APS solution and stirring at 5 °C. Finally, the PANI NS was purified by Soxhlet extraction. H_2PtCl_6 and $Ni(CHCOO)_2$ were used as precursors for Pt and Ni NPs, and both solutions and PANI were added to the GO suspension and microwaved for 120 s, then isolated by centrifugation. The collected final product was redispersed in EtOH, and 5 μL of the prepared nanozyme was deposited on the surface of a GCE. The proposed nanozyme-based sensor, rGO/PANI@PtNi/GCE, was employed for the determination of H_2O_2, and a linear concentration range was obtained between 0.1 and 126.4 mM, with a LOD of 0.5 μM. The selectivity and analytical application studies were not specified.

An immunosensor based on SWCNTs-GQDs on AuNPs-rGO[121] was prepared to immobilize the antibody anti-CEA, capable of determining CEA, as low as 5.3 pg mL^{-1}, with very good results when tested in human serum samples. A Co_3O_4–CuNi/rGO composite[126] was developed by the 2-step hydrothermal method and deposited on top of a GCE to detect AA, an essential vitamin. The linear range exhibited by the AA sensor ranged from 10 to 100 μM, and the LOD was 0.34 μM.

The Co_3O_4–CuNi–rGO/GCE was employed to detect AA from tablets, orange, and vitamin water samples, with 99.2–101.3% recovery percentages.

In a recent study, a single-step-synthesized AgNPs-rGO nanocomposite was modified with myoglobin (Myb) protein, in 2020,[120] for the simultaneous detection of two puberty biomarkers, luteinizing and follicle-stimulating hormones (LH and FSH). The nanocomposite was mixed with paraffin oil to form a homogeneous paste for the design of a nanozyme carbon paste electrode (CPE). The LOD values for the stochastic response obtained with the Myb-AgNPs-rGO CPE were 2.0 pg mL^{-1} for LH and 1.0 pg mL^{-1} for FSH. The biosensor was used for the determination of both biomolecules from saliva samples from obese and normal-weight children, and the results were similar to the ones obtained with ECLIA standard method.

From the natural biopolymers class, persimmon tannin (PT) is an eco-friendly biopolymer with multiple hydroxylic ends.[140] PT displays increased affinity towards Au, Pt, and Pd by chelating reaction; thus, the adsorption of Me^+ is effective.[141] PT is known for its ability to adsorb on the surface of GR by electrostatic and π–π interactions to prevent rGO conglomeration, being better for loading additional guest molecules.[141,142] In 2018, a nanozyme-based sensor that used PT and Pt NPs to form a nanocomposite with rGO was reported as a biosensor for the analysis of H_2O_2 from human serum samples.[105] To prepare the biosensor, the PT was added to a GO dispersion and sonicated to gain a well-dispersed PT-rGO suspension. An H_2PtCl_6 solution, as PtNPs precursor, was added to the system and stirred for 20 h. Lastly, the precipitates were redispersed in ultra-pure water to form the PT-Pt-rGO nanocomposite. The surface of an SPCE was loaded with AuNPs by the electrodeposition technique, followed by drop-casting of 18 μL from the water-dispersed nanocomposite. The designed nanozyme biosensor was employed for the analysis of H_2O_2 in a linear concentration range from 1.0 to 100.0 μM with a calculated LOD of 0.026 μM. The biosensor's response toward H_2O_2 appeared very quickly, in 3 seconds. No current modifications occurred when AA, UA, DA, and DOPAC solutions were added to the system. The proposed biosensor showed satisfactory recovery rates, from 98.4% to 108.9%, when tested in human serum samples.

Boehmite (γ-AlOOH) is one of the significant hydrated aluminas and is widely used in catalysis. It has been reported that γ-AlOOH/rGO is a favorable substrate due to its exceptional features, including outstanding electrochemical features and a large number of hydroxyl end-groups.[143] In 2017, Zhao *et al.*[106] reported boehmite NTs-rGO as a loading support for AgNPs used for the design of a nanozyme-based sensor for the determination of H_2O_2. The boehmite NTs-rGO was prepared by adding sodium aluminate to water-dispersed GO, under stirring, followed by the addition of CTAB, stirring, and an autoclave process. The product was redispersed in water and sonicated with a solution of $AgNO_3$ as the precursor for the AgNPs. The final product was dried under vacuum and then dispersed in CS, and then the suspension was used to modify the surface of a GCE to form the Ag-boehmiteNTs-rGO/GCE. The sensor displayed a linear concentration domain for the detection of H_2O_2 in the range of 5.0×10^{-7}–1.0×10^{-2} M with a LOD of 1.7×10^{-7} M (S/N = 3) and a sensitivity of 80.1 μA mM^{-1} cm^{-2}. No interferences were noticed in the company of 1 mM EtOH, glucose, and UA. The recovery rates were from 98.5% to 100.2%, which showed a reliable method for detection from disinfectant samples.

Perovskite oxides (POs) with the ABO_3 formula have become a non-noble Me choice intensively studied as a catalyst in O_2-related reactions. The O^{2-} conductivity and the O_2 vacancies present in the P structure can be individualized by integrating diverse Me oxides.[144] In 2017, He and coworkers[107] used the following oxide, $La_{0.6}Sr_{0.4}CoO_{3-\delta}$ (LSC), as nanozyme material to increase the catalytic ability of rGO for the detection of H_2O_2 and glucose. The LSC was prepared by using a combined EDTA–citrate complexing sol–gel process. LSC and rGO catalyst ink was prepared by mixing them with 5% Nafion and DI water. To form the sensor, a few μL were dropped on the surface of a GCE (d = 4 mm). The LSC-rGO/GCE was tested for the determination of H_2O_2 and glucose, showing sensitivities of 500 and 330 μA mM^{-1} cm^{-2}, respectively. The linear concentration ranges were between 0.2 μM and 3.3 mM and between 2 μM and 3.3 mM, with LOD values of 0.05 μM and 0.063 μM for H_2O_2 and glucose, respectively. No applicability studies were specified.

A bimetallic-rGO nanocomposite, based on Pd-AuNPs, was reported by Chen *et al.*,[112] for the design of a nanozyme-based sensor, in which even though the electrochemical signal was lower than the single-metal nanoparticles-rGO, its sensitivity toward the redox reaction of CAT, HQ, and RC was higher. The sensor was fabricated using electrochemical deposition, using CV in the range of 1.5 to −1.5 V, starting from GO, $PdCl_3$, and $HAuCl_4$, as a mixture of precursors. The fabricated Au–Pd nanoflowers-rGO/GCE was evaluated in different concentrations of HQ and CAT, and the linear response ranged from 1.6 μM to 0.1 mM and from 2.5 μM to 0.1 mM with LOD values of 0.5 μM and 0.8 μM, respectively. When tested in tap, lake, and river waters, the sensor exhibited good results, with recovery values from 96% to 106.5% for HQ and from 98.0% to 103.5% for CAT.

Au–$Ni(OH)_2$ nanocomposites supported on rGO (Au/Ni $(OH)_2$–rGO)[113] were prepared *via* the wet-chemical method using a mixture of GO suspension, PVP, $HAuCl_4$, $NiSO_4$, and melamine. The addition of 2 mL of $NaBH_4$ to the mixture was done under stirring. For comparison, Au/rGO, $Ni(OH)_2$/rGO, and rGO were prepared similarly. In the end, the products were centrifuged, washed, and dried in a vacuum. The Au/Ni $(OH)_2$–rGO nanozyme material was deposited on a GCE to perform the electrochemical detection of CAT. The level of CAT displayed a direct proportional behavior with its response current from 4.0×10^{-7} M to 3.4×10^{-5} M with a LOD of 1.3×10^{-7} M. After 40 days, the electrode retained 96.34% of its original response. When 100-fold K^+, Na^+, Cl^-, Cu^{2+}, I^-, NO_3^-, Trp, Tyr, and GLU were added to the system, they did not interfere with the determination of CAT when the nanozyme Au/Ni

$(OH)_2$–rGO-based electrode was employed for the measurements. The recovery percentages of CAT from lake water samples were between 94.8% and 103.8%.

Functionalized graphene composites as nanozymes for electrochemical sensing

In 2015,[145] GR was functionalized with tryptophan (Trp) for the analysis of HQ and CAT from real tap-water samples. The nanocomposite was formed by ultrasonication of 20 mg Trp in formic acid and 5 mg graphene for several hours. 6 μL of Trp-GR water dispersion was drop-cast on top of a GCE and left to dry in the air to form the proposed sensor. The ΔE_p between HQ and CAT at the Trp-Gr/GCE was 104 mV. The linear concentration range for HQ was 5–300 μM and for CAT was 5–500 μM, with LOD values of 0.22 μM for HQ and 0.09 μM for CAT, as tabulated in Table 4. The authors investigated the selectivity and found that 1000-fold HPO_4^{2-}, K^+, $H_2PO_4^-$, Ac^-, Na^+, NO^{3-}, SO_4^{2-}, Cu^{2+}, Mg^{2+}, 100-fold excess of Fe^{3+}, Ca^{2+}, Cl^-, and GLU; and 10-fold AA and UA caused a decrease in the signal of less than 5%. The recoveries from tap water containing added amounts of both analytes were 97.7–99.5% and 101.0–102.7% for HQ and CAT, respectively, proving the detection of both isomers in water at the Trp-Gr/GCE.

In another study,[146] bimetallic Au@PtNP/GO was used by Ko *et al.* to design a nanozyme platform. The synergetic effect between bimetallic nanoparticles and graphene oxide resulted in a reliable nanozyme design. Au@PtNP/GO nanozymes were obtained by functionalizing 5 mL of agarose microbeads with (3-aminopropyl)triethyloxysilane for 15 hours at room temperature and flowed by centrifuging and washing steps. Then this solution was mixed with 1.5 mL of 100 mM EDC in MES buffer (0.05 M, pH 5) and 5 mL of GO solution, which was 1 g L^{-1}. After 3 hours of stirring, the authors observed GO microbeads of intense brown color. The resulting solution was mixed with 0.9 mM $HAuCl_4$ solution and incubated for 10 min in a 60 °C water bath. For further steps, 150 mM sodium citrate was added and stirred for 2 hours at 60 °C as a reducing agent. Finally, 1 mM (aq) of H_2PtCl_6 was added to the latest mixture and mixed for 10 minutes in a hot water bath. By the addition of 10 mM of L-ascorbic acid, the Pt reduction was achieved and resulted in dark purple-colored microbeads (Fig. 11). The resulting solution was centrifuged with DI water and stored at 4 °C. The authors further characterized samples using FE-SEM, XRD, FTIR, and UV-vis studies. The authors took advantage of Pt nanoparticles' peroxide-like activity and the graphene oxides' highly oxygenated functional moieties on their surface to detect H_2O_2 with the suggested nanozyme. Compared with the HRP enzyme, Au@PtNP/GO microbeads had a lower K_m of 0.138 mM than the HRP enzyme (3.7 mM), indicating that the suggested nanozymes could be a valuable alternative to HRP. Under the optimized conditions, linear chronoamperometric responses between 1 μM and 0.1 mM H_2O_2 were obtained, with a LOD value of 1.62 μM. Moreover, the determination of H_2O_2 from artificial urine samples was achieved with recovery values between 106 and 108%. The selectivity studies were also successfully achieved using current responses of 0.1 mM H_2O_2 in the presence of 1.0 mM GLU, DA, Cys, 0.2 mM AA, and 0.5 mM AU.

In an alternative study by Mao[147] *et al.*, poly(4-vinylphenylboronic acid)-functionalized polypyrrole/GO nanosheets were suggested as a nanozyme platform for the detection of CAT and HQ. GO and polypyrrole/GO nanosheets were obtained by

Table 4 Some selected functionalized graphene composites as nanozymes for electrochemical sensing

Nanozymes	Substrate	Method	Transducer	Medium	Linear range	LOD	Application	Ref.
Tryptophan-functionalized Gr	HQ CAT	DPV	GCE	0.1 M PBS (pH 7.0)	5–300 μM 5–500 μM	0.22 μM 0.09 μM	Tap water	145
Au@PtNP/GO microbeads	H_2O_2	AMP	ITO	pH 4.0 buffer solution	1–3000 μM	1.62 μM	Artificial urine	146
P4VPBA/PPy/GO nanosheets	CAT HQ	DPV	GCE	0.05 M PBS (pH 9.0)	7–16 μM 4–22 μM	0.96 μM 0.53 μM	Tap water	147
AgNp @ Gr nanoribbons	H_2O_2	AMP	SPCE	PBS (pH 7.8)	50–5000 μM	20 μM	Milk	148
LaCo/Gr nanosheets	CAT	DPV	GCE	0.05 M PBS (pH 7.0)	0.009–132 μM	0.001 μM	NS	149
3D N–Co-CNT @ nitrogen-doped Gr	H_2O_2	AMP	GCE	0.1 M NaOH	2.0–7449 μM	2.0 μM	Human serum	150
PdPt NCGs/SnO_2/Gr nanosheets	H_2O_2	AMP	GCE	0.1 M PBS (pH 7.4)	1–300 μM	0.3 μM	Human serum	151
3D Gr walls/Cu_2O	Glucose	AMP	CFP	50 mM NaOH	0.5–5166 μM	0.21 μM	Human blood serum	152
Nitrogen-doped functionalized graphene/Pd/NiAl-LDH	Glucose	AMP	GSE	0.1 M NaOH	0.5–10 000 μM	0.234 μM	Human serum and plasma	153
3D Ni_3N/graphene aerogels	Glucose	AMP	GCE	0.1 M NaOH	0.1–7645.3 μM	0.04 μM	Human blood serum	154
3D nitrogen-doped holey graphene hydrogel/$NiCo_2O_4$ NFs	Glucose	AMP	GCE	0.1 M NaOH	5–10 950 μM	0.39 μM	Human serum	155
Porous graphene	H_2O_2	AMP	GCE	0.05 M NaOH	0.1–30 μM	0.02 μM	NS	156
Bi_2WO_6@Gr nanoribbons	CAT HQ	DPV	SPCE	PBS (pH 7.0)	0.021 – 1550 μM	0.00531 μM 0.00751 μM	Red wine and face cream	157
MOF $[Cu_2(OH)_3NO_3$@ZnO]-Gr fibers	H_2O_2	AMP	Flexible electrodes from fibers	PBS (pH 7.4)	1.00–17 400 μM	1.00 μM	Human colon cells	158

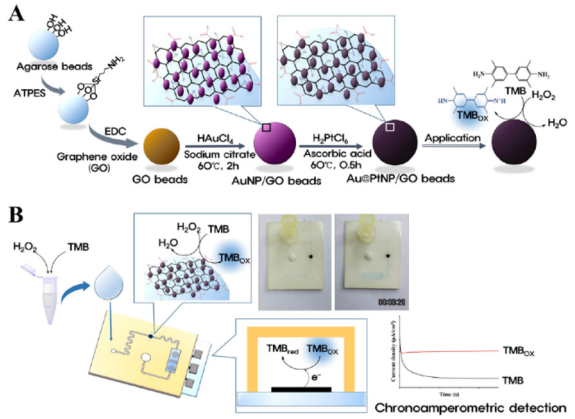

Fig. 11 Schematic diagram of (A) the preparation of Au@PtNP/GO microbeads and (B) H_2O_2 detection on electrochemical POC devices with Au@PtNP/GO nanozymes (reprinted from ref. 146, with permission from Elsevier Publisher).

the Hummers method, and polymerization of 4VPBA was achieved on the surface of PPy/GO in DMF with KOH. 1 mg of P4VPBA/PPy/GO nanosheets was dissolved in 1 mL of EtOH to prepare P4VPBA/PPy/GO suspension. From this suspension, 3 μL was dropped onto the top of GCE and used as the WE. Moreover, PPy/GO-modified GCE was also prepared for comparison studies. Characterization of each modification step was achieved by SEM, TEM, FTIR, UV-vis, XPS, and TGA studies. Between 7 and 16 μM catechol, the linear range was obtained with a LOD value of 0.96 μM, as shown in Table 4; for hydroquinone, a linear range was obtained from 4 to 22 μM with a LOD value of 0.53 μM. Interference studies were performed in the presence of 100-fold Na^+, Mn^{2+}, K^+, Ca^{2+}, Mn^{2+}, Cu^{2+}, NO^{3-}, Fe^{3+}, CO_3^{2-}, Cl^-, SO_4^{2-}, Br^-, and 50-fold tartaric acid, CA, AA, Ph, and 20-fold RC, UA. The authors stated that the detection error was less than 2.6%, indicating no interfering effect of these substances.

Moreover, the authors also performed repeatability, reproducibility, and stability studies. Using DPV, repeatable and reproducible results for 10 μM CC and 10 μM HQ were obtained with lower than 1% RSD values. When the nanosensor was maintained at 5 °C for one week, there was no change in the peak potential related to catechol and hydroquinone. Real sample applications were also performed in tap water, with recovery values between 97 and 107%.

In another study that was accomplished by Xue[159] *et al.*, Pd nanoparticles and porous graphene (PGR) were used to prepare a nanozyme platform for the detection of H_2O_2. Firstly, 1.6 mg of ZnONPs and 1 mL of 0.8 mg L^{-1} GO were ultrasonicated for 2 h and stirred for 12 hours at 24 °C. Furthermore, 0.02 mL poly(diallyldimethylammonium chloride) (PDDA) was additionally introduced into the solution. 10 μL of PDDA/ZnO/GO was drop-cast on the GCE, and this GCE was immersed in $NaBH_4$ for 12 hours, and the reduction of $PdCl_4^{2-}$ and GO was accomplished. Then to remove the ZnO, the modified GCE was immersed in 2 M HCl. The characterization of Pd/PDDA/PGR was achieved by SEM, XRD, XPS, and X-ray analysis. Compared with the PDDA/GO, PDDA/ZnO/GO, PDDA/ZnO/GR, PDDA/GR, and PDDA/PGR using Pd/PDDA/PGR, a positive shift in the response of H_2O_2 was observed due to the excellent catalytic properties of the Pd nanoparticles' synergetic effect between Pd and the PGR. With successive additions of H_2O_2 at the potential of −0.20 V a linear range was obtained from 2 to 1672 μM H_2O_2 with a LOD value of 0.9 μM. The sensitivity was also calculated as 57.7 μA mM^{-1}.

In 2018, Rajaji *et al.*[157] suggested a nanozyme platform based on a Bi_2WO_6 flowers-decorated graphene nanoribbon (GONR) composite for the electrochemical sensing of hazardous dihydroxybenzene isomers, catechol, and hydroquinone. The authors used microwave-assisted synthesis instead of the classical hydrothermal method, indicating that this is a cost-effective alternative method. Firstly, graphene nanoribbons were obtained by the unzipped MWCNTs preparation strategy. Then the synthesized graphene nanoribbons were redispersed in water, and $Na_2WO_4{\cdot}2H_2O$ and $Bi(NO_3)_3{\cdot}5H_2O$ were added to the suspension. The mixture was transferred to the microwave and exposed to microwave radiation for 30 min at 160 °C with vigorous stirring. After collecting the precipitate from centrifugation at 6000 rpm, the powder was further calcinated. 1 mg of this powder was dissolved in 1 mL of water/ethanol mixture, and 6 μL from this dispersion was drop-cast added on top of the SPCE (Fig. 12). DPV studies were performed for the determination of catechol and hydroquinone. Within a broad linear range between 21 nM and 1550 μM, hydroquinone was determined with a LOD value of 7.51 nM. The sensitivity of the nanozyme towards hydroquinone was found as 42.2 μA μM^{-1} cm^{-2}. For the determination of catechol, a linear range was obtained from 21 nM to 1550 μM, with a sensitivity of 54.14 μA μM^{-1} cm^{-2}. The proposed nanozyme exhibits a low detection limit of 5.31 nM, as reported in Table 4. For real sample applications, the authors successfully reported recovery % values related to pharmaceutical face cream and water samples without any pre-treatment or separation procedures.

In a very recent study, Stanković *et al.*[148] suggested a nanozyme based on silver nanoparticle and graphene nanoribbon (AgNp@GNR) nanocomposites for the electrochemical detection of H_2O_2. The AgNp@GNR was synthesized basically by mixing 2 mL of AgNP and 10 mL of GNR (10 mg per 10 mL). Then this solution was sonicated for 15 min and left at room temperature for 12 h, then centrifuged, followed by washing steps. From the solid part, 5 mg was dissolved in 1 mL di-

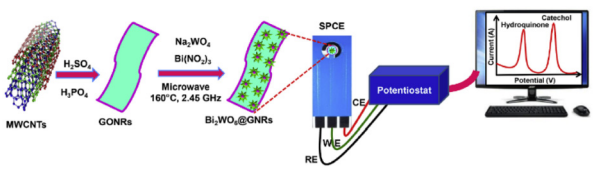

Fig. 12 Schematic illustration for the preparation of Bi_2WO_6@GNRs nanocomposite for sensing dihydroxybenzene isomers in water samples and face cream sample. WE = working electrode, RE = reference electrode, CE = counter electrode (reprinted from ref. 157 with permission from Elsevier Publisher).

methylformamide and sonicated for 3 hours. From this composite, 5 μL was dropped on SPCE and used in the detection of H_2O_2. The analytical parameters, such as pH value of supporting electrolyte and operating potential, were optimized, and chronoamperometric measurements were used for the determination of H_2O_2. From 0.05 to 1.8 mM H_2O_2 linear range with a LOD value of 20 μM, H_2O_2 detection was achieved. The authors also reported that the nanozyme-modified sensor maintained its activity of 92.3% for 5 weeks. For real sample applications, the authors used the standard addition method for the detection of H_2O_2 concentration in milk samples, and with acceptable recoveries between 96.0 and 104.0% the real sample analyses were achieved.

In 2020, Suvina *et al.*[149] designed a nanozyme for the electrochemical detection of catechol using La cobaltite maintained on GR nanosheets (LaCo/GNS). The authors took advantage of the synergetic effect between graphene nanosheets and lanthanum cobaltite, as they display excellent electron transfer, high biocompatibility, numerous amounts of active sites, strong adsorption ability, and increased conductivity due to their narrow bandgap (0.5–0.6 eV). 8 μL of LCO/GNS suspension was cast onto the top of the GCE and dried at 24 °C. A calibration plot was obtained from 0.009 to 203 μM catechol with a LOD value of 1 nM. The reproducibility studies were performed from 4 different electrodes, and repeatability studies were performed with eight consecutive measurements of 200 μM catechol. Low RSD values related to reproducibility and repeatability were obtained. Moreover, the effect of various interferences such as hydroquinone, acetaminophen, uric acid, isoniazid, and salicylic acid was tested, and the authors reported that the detection of CAT was not affected by these interferences. For a real sample application, river water from Taipei was used with a basic sample filtration method to remove impurities. Acceptable % recoveries were obtained between 96.25 and 98.75%, indicating the potential use of this nanozyme in real sample applications.

In their study, Balamurugan[150] *et al.* proposed a novel hierarchical 3D N–Co-CNT@NG nanocomposite as a nanozyme for the analysis of GLU and H_2O_2. The synthesis of N–Co-CNT@NG nanocomposite was started from cyanamide and $(CH_3COO)_2Co{\cdot}4H_2O$ (1 mM), which were dissolved in 10 mL of deionized water and mixed well. Then 120 mL of 2 mg mL^{-1} GO was added to the solution and ultrasonicated for 2 h, followed by stirring for 6 h. After gradual evaporation at 80 °C and further purification steps, the final mixture was centrifuged and washed several times to obtain a 3D N–Co-CNT@NG nanocomposite. The synthesized nanocomposite was well characterized by FE-SEM, TEM, X-Ray, XRD patterns, Raman, and BET measurements. 1 mg of 3D N–Co-CNT@NG nanocomposite was prepared in 1 mL DMF, ultrasonicated for 30 min and used to modify the surface of the glassy carbon electrode. A standard three-electrode system formed from a GCE as a WE, Ag/AgCl electrode as a RE, and a Pt foil as a CE was used for the determination of glucose and H_2O_2. To achieve an oxygen-free medium, nitrogen was used to purge the solution. After pH, potential, and volume optimization studies, glucose detection was achieved from 0.025 to 10.83 mM glucose at a potential of +0.32 V with a high sensitivity of 9.05 μA mM^{-1} cm^{-2}. Moreover, LOD was calculated as 100 nM. The interference studies were performed through commonly interfering ions such as AA and UA that usually coexist in human blood with glucose. The interference results were negligible, indicating a selective nanozyme platform as suggested by the authors. For H_2O_2 detection, a LOD value of 2.0 μM was obtained within a linear range of 2.0 μM to 7.449 mM at −0.04 V. In selectivity studies, glucose was also added beside ascorbic acid and uric acid; yet again, negligible current responses were obtained, which indicates these ions do not inhibit the detection of H_2O_2. Hence the authors stated that the 3D N–Co-CNT@NG nanozyme could be used in different areas, including medical, environmental, and electrochemical fields.

In another interesting study, GR blended with SnO_2 and Pd–Pt nanocages (PdPt NCs@SGN) composites were prepared for the electrochemical detection of H_2O_2 released from living cells.[151] SGN nanosheets were prepared using a one-step hydrothermal process, and the PdPt NCs@SGN nanocomposite was prepared from the starting materials of polyvinylpyrrolidone, ascorbic acid, and KBr in 8 mL ultrapure water with heating at 80 °C in an oil bath for 10 min. Following that, K_2PdCl_4 was added to the medium and refluxed for 3 h at 80 °C. With the same strategy, by adding K_2PtCl_4 to this solution, PdPtNCs were prepared. 5 mg of SGN mixed with 5 mL of PdPtNCs and ultrasonicated for 2 hours. The surface of the GCE was modified with 10 mL of PdPtNCs suspension and used as the WE in the 3-electrode system. H_2O_2 detection was achieved at −0.1 V in pH 7.4, 0.1 M PBS with linear concentration levels of 1–300 μM with a LOD value of 0.3 μM, as tabulated in Table 4. Recovery studies were performed from human serum samples, with mean recoveries between 98.94 and 104.18%. Moreover, the authors achieved a real application for detecting H_2O_2 released from living cells.

Glucose is the most important and intensively studied biomarker in the diagnosis of diabetes. Nowadays, there are several commercially available sensors for glucose monitoring, and research in this area is challenging but also a requirement to advance this field. Graphene-nanozyme-based electrochemical sensors[127,152–154] have been reported as highly sensitive sensors for glucose detection in biological samples.

In 2020, Yang and coworkers[152] reported carbon fiber paper (CFP) as a substrate for the design of a sensitive glucose sensor. The CFP was modified with a 3D GR wall (GWs) and Cu_2ONPs as sensing layers for glucose detection. The GR was grown vertically on the CFP by RF-PECVD to obtain a uniform film of layered GWs. The CFP/GWs were then covered with Cu_2ONPs that were gained by complete thermal decomposition of $Cu(CH_3COO)_2$. After that, the CFP/GWs/Cu_2O was cut into pieces of 0.7 × 0.7 cm^2, and the CFP/GWs/Cu_2O sensor was effectively obtained. The linear concentration range for glucose detection was between 0.5 and 5166.0 μM, and the LOD was 0.21 μM.

Shishegari *et al.*[153] reported a glucose sensor that was prepared in only one electrochemical deposition procedure, forming Pd-NiAl-LDH, that was deposited on a graphite sheet electrode (GS) covered by N-GR. The exceptional features of LDHs, such as layered structure, ionic exchange compatibility, high surface area, catalytic activity, and low cost, make these materials perfect candidates for electrochemical sensing applications.[160] Owing to the superior properties of NiAl-LDH, rapid electron exchange can be reached due to the presence of Ni active sites in its structure,[153] and it generates a fascinating material for use as a nanozyme sensing layer. The design of the proposed sensor was obtained by the deposition of N-GR to coat the GS electrode, followed by the electrodeposition of Pd-NiAl-LDH film using the CA technique at a constant potential of −0.9 V (*vs.* Ag/AgCl) in a mixture containing $PdCl_2$, Ni $(NO_3)_2$, Al(NO_3) HNO_3, and KNO_3 solutions. The fabricated Pd-NiAL-LDH-N-GR/GS was tested using the LSV technique in a solution containing different concentrations of glucose, and linearity was obtained in the range of 0.5 μM–10.0 mM, and the LOD value was 0.2 μM. After a storage period of 1 month, the sensor showed about 90% of its initial response current.

Yin and coworkers[154] reported a glucose sensor based on the functionalization of a GCE with Ni_3N NPs on conductive 3D graphene aerogels (GA). Intensively studied, 3D GA is a 3D graphene-based architecture, which is a valuable nanomaterial because it limits the aggregation issue of graphene layers and improves the electrocatalytic activity by offering more active sites.[154] The Ni_3N-GA was manufactured by a hydrothermal method, followed by a freeze-drying process, and calcinated under an NH_3 atmosphere (Fig. 13).

As a glucose sensor, the nanozyme-based Ni_3N-GA/GCE provided linear detection levels of 1.0×10^{-7}–7.6×10^{-2} M, and the calculated sensitivity was 905.6 mA mM^{-1} cm^{-2}, and the LOD value was 0.04 μM.

The fabrication of a 3D N-doped holey GR hydrogel decked with $NiCo_2O_4$ NFs (NHGH/$NiCo_2O_4$) was described in 2019.[155] The single-phase binary $NiCo_2O_4$ with a characteristic spinel structure showed increased conductivity due to its multiple oxidation states.[161] The nanocomposite material was deposited on top of a GCE to form a glucose sensor and H_2O_2 sensor exhibiting linear concentration levels (GLU: 5.00×10^{-6}–1.09×10^{-4} M; H_2O_2: 1.0×10^{-6}–5.1×10^{-6} M), with LODs for GLU: 0.39 μM and for H_2O_2: 0.136 μM.

All these papers[127,152–154] reported very good applicability and selectivity of the nanozyme GR-based sensors in serum samples for GLU determination. However, the lowest detection limit and wide concentration range were reached with the Ni_3N NPs loaded on a 3D structured GA, proving that the 3D architecture of graphene is an outstanding support material in the design of nanozyme-based sensors.

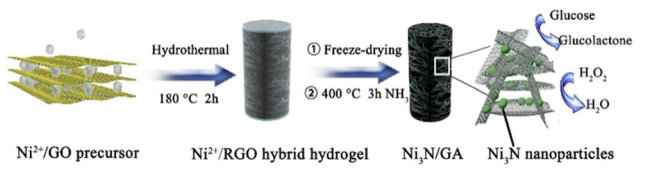

Fig. 13 Illustration of the preparation of Ni_3N/GA samples (reprinted with permission from ref. 154).

Conclusions and future perspectives

The use of GR-based nanozymes in sensor development is gaining momentum due to their enhanced electron-transfer kinetics, high surface-to-volume ratios, easy functionalization, high stability, low cost, and biocompatibility. GR-based nanozymes possess unique nanomaterial properties, providing a multiplex platform that can bond with complex biochemical environments, making them an attractive substitute for enzymes in biosensors. However, their catalytic ability can still be improved, along with their selectivity. These two features, selectivity and catalytic ability, are the most important parameters for nanozyme platforms to be competitive with enzymatic biosensors. The functionalization of graphene-based nanomaterials with different nanoparticles can enhance their nanozymatic features, as mentioned in this review. Graphene oxide functionalization presents a promising approach for creating nanozymes that can mimic various natural enzymes. To achieve this, researchers may integrate nanozyme-based assay platforms with technological transducers like smartphones, and it is believed that combining these platforms with portable devices and other advanced technologies will be a promising direction in the analytical field. Interdisciplinary efforts are required to develop a potential nanozyme-based detection system.

One of the most exciting future prospects for nanozyme-based detection systems is their integration with artificial intelligence (AI) and machine learning (ML) algorithms. The combination of nanozymes with AI/ML algorithms will enable highly sensitive and specific detection of target analytes, even in complex matrices. The integration of these technologies will also enable the development of smart sensors that can adapt to changing environments and provide real-time feedback.

Another future direction for nanozyme-based detection systems is the development of multifunctional sensors that can detect multiple analytes simultaneously. Such sensors will have significant implications in the fields of medical diagnostics, environmental monitoring, and food safety, where the detection of multiple targets is often required.

Furthermore, the development of nanozyme-based therapeutics is an exciting prospect for the future. Nanozymes have shown promise in various biomedical applications, including cancer therapy, drug delivery, and wound healing. The integration of nanozymes with other nanomaterials and drug molecules could lead to the development of highly efficient and targeted therapeutics.

Overall, the future of nanozyme-based detection systems and therapeutics is highly promising, with many exciting opportunities for interdisciplinary research and development. Integrating these systems with advanced technologies and AI/

ML algorithms will enable highly sensitive and specific detection and treatment of various diseases and conditions.

Abbreviations

Ab1	Primary antibody
Ab2	Secondary antibody
ABS	Acetate buffer solution
AMP	Amperometry
APTES	(3-Aminopropyl)triethoxysilane
BDD	Boron-doped diamond
Bi_2WO_6	Bismuth tungstate
BRB	Britton Robinson buffer
BSA	Bovine serum albumin
BTC	1,3,5-Benzenetricarboxylic acid
CAT	Catechol
CBS	Citrate buffer solution
CDs	Carbon dots
CEA	Carcinoembryonic antigen
c-MWCNT	Carboxylated multi-walled carbon nanotubes
CNTs	Carbon nanotubes
COF	Covalent organic framework
$CoNiO_2$	Cobalt nickel oxide
Cp	Coordination polymer
CS	Chitosan
CTAB	Cetyl trimethyl ammonium bromide
Cu-Cys	Copper(II) complex of cysteine
CV	Cyclic voltammetry
Cys	Cysteine
DPAV	Differential pulse anodic voltammetry
DPV	Differential pulse voltammetry
EIS	Electrochemical impedance spectroscopy
ERGO	Electrochemically reduced graphene oxide
Fc	Ferrocene carboxylic acid
FPBA	2-Fluorophenylboronic acid
GCE	Glassy carbon electrode
GCN	Graphene-like carbon nanosheets
GO	Graphene oxide
Gr	Graphene
GS	Graphene sheets
GSE	Graphite sheet electrode
HA	Hydroxyapatite
His	Histidine
HQ	Hydroquinone
IL	Poly ionic liquid
ITO	Indium tin oxide
LSV	Linear sweep voltammetry
Mil	McIlvaine buffer
MIPs	Molecularly imprinted polymers
MOF	Metal organic framework
MWCNTs	Multi-wall carbon nanotubes
Nf	Nafion
NFG	Nitrogen-doped functionalized graphene
NFs	Nanoflowers
NG	Nitrogen-doped graphene
N-HMCS	Nitrogen-doped hollow mesoporous carbon spheres
NiAl-LDHs	NiAl layered double hydroxides
NRs	Nanorods
NS	Not stated
NSs	Nanosheets
NTs	Nanotubes
P4VPBA	Poly(4-vinylphenylboronic acid)
PAMAM	Poly(amidoamine) dendrimer
PANI	Polyaniline
PB	Prussian blue
PBA	Prussian blue analog
PBS	Phosphate buffer solution
PDA	Polydopamine
PDDA	Poly(diallyldimethylammonium chloride)
PEDOT	Poly(3,4-ethylenedioxythiophene)
PEI	Polyetherimide
PG	Pencil graphite
PGE	Pencil graphite electrode
PN	Porphyrin
POM	Phosphomolybdic acid hydrate
PPy	Polypyrrole
pRGO	Partially reduced graphene oxide
PT	Persimmon tannin
QDs	Quantum dots
rGO	Reduced graphene oxide
SGN	SnO_2/graphene nanosheets
SPCE	Screen printed carbon electrode
SWCNTs	Single-walled carbon nanotubes
SWV	Square wave voltammetry
TCPP	Tetra(4-carboxyphenyl)porphine
β-CD	β-Cyclodextrin

Author contributions

Livia Alexandra Dinu: conceptualization, writing – original draft, writing – review & editing, visualization; Sevinc Kurbanoglu: conceptualization, writing – review & editing, visualization.

Conflicts of interest

There are no conflicts to declare.

Acknowledgements

This work was supported by a grant from the Ministry of Research, Innovation and Digitization, CNCS – UEFISCDI, core project number 2307 "Advanced research in micro–nano electronic and photonic devices, sensors and microsystems for societal applications" within PNCDI IV (2022–2027) and contract no. PFE541 "Strengthening IMT Excellence in MicroNano Advanced Technologies (MicroNEx)".

References

1 A. M. Baracu and L. A. D. Gugoasa, *J. Electrochem. Soc.*, 2021, **168**, 037503.
2 I. H. Cho, D. H. Kim and S. Park, *Biomater. Res.*, 2020, **24**, 1–12.
3 X. Li, L. Wang, D. Du, L. Ni, J. Pan and X. Niu, *TrAC, Trends Anal. Chem.*, 2019, **120**, 1–13.
4 L. Gao, J. Zhuang, L. Nie, J. Zhang, Y. Zhang, N. Gu, T. Wang, J. Feng, D. Yang, S. Perrett and X. Yan, *Nat. Nanotechnol.*, 2007, **2**, 577–583.
5 B. Garg and T. Bisht, *Molecules*, 2016, **21**, 1–16.
6 R. G. Mahmudunnabi, F. Z. Farhana, N. Kashaninejad, S. H. Firoz, Y. B. Shim and M. J. A. Shiddiky, *Analyst*, 2020, **145**, 4398–4420.
7 D. Jiang, D. Ni, Z. T. Rosenkrans, P. Huang, X. Yan and W. Cai, *Chem. Soc. Rev.*, 2019, **48**, 3683–3704.
8 Q. Wang, H. Wei, Z. Zhang, E. Wang and S. Dong, *TrAC, Trends Anal. Chem.*, 2018, **105**, 218–224.
9 Y. Huang, J. Ren and X. Qu, *Chem. Rev.*, 2019, **119**, 4357–4412.
10 J. Wu, X. Wang, Q. Wang, Z. Lou, S. Li, Y. Zhu, L. Qin and H. Wei, *Chem. Soc. Rev.*, 2019, **48**, 1004–1076.
11 Y. Zhang, S. Li, H. Liu, W. Long and X. D. Zhang, *Front. Chem.*, 2020, **8**, 1–13.
12 M. Sharifi, S. H. Hosseinali, P. Yousefvand, A. Salihi, M. S. Shekha, F. M. Aziz, A. JouyaTalaei, A. Hasan and M. Falahati, *Mater. Sci. Eng., C*, 2020, **108**, 110422.
13 W. Dong, Y. Zhuang, S. Li, X. Zhang, H. Chai and Y. Huang, *Sens. Actuators, B*, 2018, **255**, 2050–2057.
14 M. H. M. Facure, R. S. Andre, R. M. Cardoso, L. A. Mercante and D. S. Correa, *Electrochim. Acta*, 2023, **441**, 141777.
15 Y. Liao, J. Liu, M. Liu, L. Lin, X. Wang and Z. Quan, *Microchem. J.*, 2023, **185**, 108184.
16 P. K. Boruah, P. Borthakur, G. Neog, B. Le Ouay, N. U. Afzal, P. Manna and M. R. Das, *ACS Appl. Nano Mater.*, 2023, **6**, 1667–1677.
17 L. A. D. Gugoasa, C. C. Negut and C. Stefanov, in *Electroanalytical Applications of Quantum Dot-Based Biosensors*, 2021, pp. 395–425.
18 R. Zhang, K. Fan and X. Yan, *Sci. China: Life Sci.*, 2020, **63**, 1183–1200.
19 H. Liang, F. Lin, Z. Zhang, B. Liu, S. Jiang, Q. Yuan and J. Liu, *ACS Appl. Mater. Interfaces*, 2017, **9**, 1352–1360.
20 J. Wu, X. Wang, Q. Wang, Z. Lou, S. Li, Y. Zhu, L. Qin and H. Wei, *Chem. Soc. Rev.*, 2019, **48**, 1004–1076.
21 X. Yan and L. Gao, in *Nanozymology: Connecting Biology and Nanotechnology*, ed. D. Lockwood, Springer US, Beijing, 2020, pp. 3–16.
22 G. Li, M. Chen, B. Wang, C. Wang, G. Wu, J. Liang and Z. Zhou, *Anal. Chim. Acta*, 2022, **1221**, 340102.
23 Z. Li, J. Zhang, G. Dai, F. Luo, Z. Chu, X. Geng, P. He, F. Zhang and Q. Wang, *J. Mater. Chem. B*, 2021, **9**, 9324–9332.
24 G. Li, B. Wang, L. Li, X. Li, R. Yan, J. Liang, X. Zhou, L. Li and Z. Zhou, *Molecules*, 2023, **28**, 2271.
25 J. Luo, D. Jiang, T. Liu, J. Peng, Z. Chu and W. Jin, *Biosens. Bioelectron.*, 2018, **104**, 1–7.
26 Z. Yu, R. Lou, W. Pan, N. Li and B. Tang, *Chem. Commun.*, 2020, **56**, 15513–15524.
27 H. Y. Mohammed, M. Farea, N. N. Ingle, T. Al-Gahouari, P. W. Sayyad, G. A. Bodkhe, M. M. M. Mahadik, S. M. Shirsat and M. D. Shirsat, *J. Electrochem. Soc.*, 2021, **168**, 106509.
28 M. A. Ali, L. Dong, J. Dhau, A. Khosla and A. Kaushik, *J. Electrochem. Soc.*, 2020, **167**, 037550.
29 R. Kour, S. Arya, S.-J. Young, V. Gupta, P. Bandhoria and A. Khosla, *J. Electrochem. Soc.*, 2020, **167**, 037555.
30 C. Li, Y. Wang, H. Jiang and X. Wang, *J. Electrochem. Soc.*, 2020, **167**, 037540.
31 S. Kumar, V. Pavelyev, N. Tripathi, V. Platonov, P. Sharma, R. Ahmad, P. Mishra and A. Khosla, *J. Electrochem. Soc.*, 2020, **167**, 047506.
32 N. Stasyuk, O. Smutok, O. Demkiv, T. Prokopiv, G. Gayda, M. Nisnevitch and M. Gonchar, *Sensors*, 2020, **20**, 1–42.
33 N. I. Zaaba, K. L. Foo, U. Hashim, S. J. Tan, W.-W. Liu and C. H. Voon, *Procedia Eng.*, 2017, **184**, 469–477.
34 R. K. Singh, R. Kumar and D. P. Singh, *RSC Adv.*, 2016, **6**, 64993–65011.
35 X. Mei, X. Meng and F. Wu, *Phys. E*, 2015, **68**, 81–86.
36 S. P. Sasikala, P. Poulin and C. Aymonier, *Adv. Mater.*, 2017, **29**(2), 1605473.
37 F. Ratto, P. Matteini, F. Rossi and R. Pini, *J. Nanopart. Res.*, 2010, **12**, 2029–2036.
38 R. Das, A. Dhiman, A. Kapil, V. Bansal and T. K. Sharma, *Anal. Bioanal. Chem.*, 2019, **411**, 1229–1238.
39 M. Cui, J. Zhou, Y. Zhao and Q. Song, *Sens. Actuators, B*, 2017, **243**, 203–210.
40 Y. Li, X. Jian, S. Zhou, Y. Lu, C. Zhao, Z. Gao and Y. Y. Song, *ACS Appl. Mater. Interfaces*, 2019, **11**, 17215–17225.
41 A. J. Kora, *IET Nanobiotechnol.*, 2019, **13**, 602–608.
42 J. Shah, R. Purohit, R. Singh, A. S. Karakoti and S. Singh, *J. Colloid Interface Sci.*, 2015, **456**, 100–107.
43 H. Gu, Q. Huang, J. Zhang, W. Li and Y. Fu, *Colloids Surf., A*, 2020, **606**, 125455.
44 S. Biswas, P. Tripathi, N. Kumar and S. Nara, *Sens. Actuators, B*, 2016, **231**, 584–592.
45 L. T. Lanh, T. T. Hoa, N. D. Cuong, D. Q. Khieu, D. T. Quang, N. Van Duy, N. D. Hoa and N. Van Hieu, *J. Alloys Compd.*, 2015, **635**, 265–271.
46 B. Unnikrishnan, C. W. Lien, H. W. Chu and C. C. Huang, *J. Hazard. Mater.*, 2021, **401**, 123397.
47 L. A. D. Gugoasa, *J. Electrochem. Soc.*, 2020, **167**, 037506.
48 X. Niu, N. Cheng, X. Ruan, D. Du and Y. Lin, *J. Electrochem. Soc.*, 2020, **167**, 037508.
49 M. Pietrzak and P. Ivanova, *Sens. Actuators, B*, 2021, **336**, 129736.
50 M. Coroș, S. Pruneanu and R.-I. Stefan-van Staden, *J. Electrochem. Soc.*, 2020, **167**, 037528.
51 P. Pang, Z. Yang, S. Xiao, J. Xie, Y. Zhang and Y. Gao, *J. Electroanal. Chem.*, 2014, **727**, 27–33.

52 P. Liu, J. Li, X. Liu, M. Li and X. Lu, *J. Electroanal. Chem.*, 2015, **751**, 1–6.
53 Y. Song, T. Yang, X. Zhou, H. Zheng and S. I. Suye, *Anal. Methods*, 2016, **8**, 886–892.
54 Z.-Y. Gao, Y.-L. Gao, E. Wang, S. Xu and W. Chen, *J. Electrochem. Soc.*, 2016, **163**, H528–H533.
55 H. Jiang, S. Wang, W. Deng, Y. Zhang, Y. Tan, Q. Xie and M. Ma, *Talanta*, 2017, **164**, 300–306.
56 S. Cotchim, K. Promsuwan, M. Dueramae, S. Duerama, A. Dueraning, P. Thavarungkul, P. Kanatharana and W. Limbut, *J. Electrochem. Soc.*, 2020, **167**, 155528.
57 S. N. A. Mohd Yazid, I. Md Isa, N. M. Ali, N. Hashim, M. I. Saidin, M. S. Ahmad, A. M. Asiri, A. Khan and R. Zainul, *Int. J. Environ. Anal. Chem.*, 2020, 1–18.
58 S. Rison, K. B. Akshaya, V. S. Bhat, G. Shanker, T. Maiyalagan, E. K. Joice, G. Hegde and A. Varghese, *Electroanalysis*, 2020, **32**, 2128–2136.
59 D. Song, J. Xia, F. Zhang, S. Bi, W. Xiang, Z. Wang, L. Xia, Y. Xia, Y. Li and L. Xia, *Sens. Actuators, B*, 2015, **206**, 111–118.
60 L. Zhang, F. Chen, G. Ren and Z. Wang, *Funct. Mater. Lett.*, 2022, **15**, 2250004.
61 E. A. Veal, A. M. Day and B. A. Morgan, *Mol. Cell*, 2007, **26**, 1–14.
62 C. Shurui, Z. Lei, C. Yaqin and Y. Ruo, *Biosens. Bioelectron.*, 2012, **42**, 532.
63 A. Ahmadalinezhad and A. Chen, *Biosens. Bioelectron.*, 2011, **26**, 4508.
64 C. Karuppiah, S. Palanisamy and S. M. Chen, *Electrocatalysis*, 2014, **5**, 177.
65 S. Liu, L. Wei, S. Guo, J. Jiang, P. Zhang, J. Han, Y. Ma and Q. Zhao, *Sens. Actuators, B*, 2018, **262**, 436–443.
66 X. Miao, C. Yang, C. H. Leung and D. L. Ma, *Sci. Rep.*, 2016, **6**, 1–8.
67 E. Goki and C. Manish, *Adv. Mater.*, 2010, **22**, 2392–3415.
68 Q. Zheng, Z. Li, J. Yang and J. K. Kim, *Prog. Mater. Sci.*, 2014, **64**, 200–247.
69 L. Zheng, Y. Chi, Y. Dong, J. Lin and B. Wang, *J. Am. Chem. Soc.*, 2009, **131**, 4564–4565.
70 J. Tang, L. Huang, Y. Cheng, J. Zhuang, P. Li and D. Tang, *Microchim. Acta*, 2018, **185**, 569.
71 Q. Zhang, Y. Hu, D. Wu, S. Ma, J. Wang, J. Rao, L. Xu, H. Xu, H. Shao, Z. Guo and S. Wang, *Talanta*, 2018, **183**, 258–267.
72 G. H. Jin, E. Ko, M. K. Kim, V. K. Tran, S. E. Son, Y. Geng, W. Hur and G. H. Seong, *Sens. Actuators, B*, 2018, **274**, 201–209.
73 X. Liu, X. Zhang and J. Zheng, *Microchem. J.*, 2021, **160**, 105595.
74 B. Ma, H. Guo, M. Wang, Q. Wang, W. Yang, Y. Wang and W. Yang, *Microchem. J.*, 2020, **155**, 104776.
75 S. Erogul, S. Z. Bas, M. Ozmen and S. Yildiz, *Electrochim. Acta*, 2015, **186**, 302–313.
76 T. Liu, B. Fu, J. Chen, Z. Yan and K. Li, *Electrochim. Acta*, 2018, **269**, 136–143.
77 M. Soltani-Shahrivar, N. Karimian, H. Fakhri, A. Hajian, A. Afkhami and H. Bagheri, *Electroanalysis*, 2019, **31**, 2455–2465.
78 S. Palanisamy, S. K. Ramaraj, S. M. Chen, T. W. Chiu, V. Velusamy, T. C. K. Yang, T. W. Chen and S. Selvam, *J. Colloid Interface Sci.*, 2017, **496**, 364–370.
79 G. Boopathy, M. Keerthi, S. M. Chen, M. J. Umapathy and B. N. Kumar, *Mater. Chem. Phys.*, 2020, **239**, 121982.
80 T. S. S. K. Naik, S. Saravanan, K. N. S. Saravana, U. Pratiush and P. C. Ramamurthy, *Mater. Chem. Phys.*, 2020, **245**, 122798.
81 S. Palanisamy, K. Thangavelu, S. M. Chen, B. Thirumalraj and X. H. Liu, *Sens. Actuators, B*, 2016, **233**, 298–306.
82 W. Zhang, L. Wang, N. Zhang, G. Wang and B. Fang, *Electroanalysis*, 2009, **21**, 2325–2330.
83 M. P. O'Halloran, M. Pravda and G. G. Guibault, *Talanta*, 2001, **55**, 605–611.
84 P. Zhu and V. Meunier, *J. Chem. Phys.*, 2012, **137**(24), 244703.
85 X. Zhang, K.-P. Wang, L.-N. Zhang, Y.-C. Zhang and L. Shen, *Anal. Chim. Acta*, 2018, **1036**, 26–32.
86 M. Shahbakhsh, S. Narouie and M. Noroozifar, *J. Pharm. Biomed. Anal.*, 2018, **161**, 66–72.
87 W. J. Grimes, *Biochemistry*, 1970, **9**, 5083–5092.
88 L. Zhu, Z. Zhong and E. V. Anslyn, *J. Am. Chem. Soc.*, 2005, **127**, 4260–4269.
89 X. Yuan, Y. Q. Tay, X. Y. Dou, Z. T. Luo, D. T. Leong and J. P. Xie, *Anal. Chem.*, 2013, **85**, 1913–1919.
90 B. Bellina, I. Compagnon, F. Bertorelle, M. Broyer, R. Antoine and P. Dugourd, *J. Phys. Chem. C*, 2011, **115**, 24549–24554.
91 W. J. Chen, L. Zheng, M. L. Wang, Y. W. Chi and G. Chen, *Anal. Chem.*, 2013, **85**, 9655–9663.
92 F. F. Cao, E. G. Ju, C. Q. Liu, F. Pu, J. S. Ren and X. G. Qu, *Chem. Commun.*, 2016, **52**, 5167–5170.
93 W. Jiang, L. Wu, J. Duan, H. Yin and S. Ai, *Biosens. Bioelectron.*, 2018, **99**, 660–666.
94 X. Fang, B. Zong and S. Mao, *Nano-Micro Lett.*, 2018, **10**, 64.
95 D. P. Nikolelis, G. Raftopoulou, N. Psaroudakis and P. G. Nikoleli, *Electroanalysis*, 2008, **20**, 1574–1580.
96 Y. Zhang, Y. Yang, L. Mao, D. Cheng, Z. Zhan and J. Xiong, *Mater. Lett.*, 2016, **182**, 298–301.
97 Y. Chen, B. Liu, Q. Liu, J. Wang, J. Liu, H. Zhang, S. Hu and X. Jing, *Electrochim. Acta*, 2015, **178**, 429–438.
98 G. Parvari, S. Annamalai, I. Borovoi, H. Chechik, M. Botoshansky, D. Pappo and E. Keinan, *Chem. Commun.*, 2014, **50**, 2494–2497.
99 C. H. Lai, M. Y. Lu and L. J. Chen, *J. Mater. Chem.*, 2012, **22**, 19–30.
100 Z. Bai, G. Li, J. Liang, J. Su, Y. Zhang, H. Chen, Y. Huang, W. Sui and Y. Zhao, *Biosens. Bioelectron.*, 2016, **82**, 185–194.
101 H. Yang, J. Zhou, J. Bao, Y. Ma, J. Zhou, C. Shen, H. Luo, M. Yang, C. Hou and D. Huo, *Microchem. J.*, 2021, **162**, 2–9.

102 P. Moozarm Nia, P. M. Woi and Y. Alias, *Appl. Surf. Sci.*, 2017, **413**, 56–65.
103 M. Wang, C. Wang, Y. Liu, B. Hu, L. He, Y. Ma, Z. Zhang, B. Cui and M. Du, *Microchim. Acta*, 2020, **187**, 436.
104 F.-G. He, J.-Y. Yin, G. Sharma, A. Kumar, F. J. Stadler and B. Du, *Nanomaterials*, 2019, **9**, 1109.
105 Y. Huang, Y. Xue, J. Zeng, S. Li, Z. Wang, C. Dong, G. Li, J. Liang and Z. Zhou, *Mater. Sci. Eng., C*, 2018, **92**, 590–598.
106 C. Zhao, H. Zhang and J. Zheng, *J. Electroanal. Chem.*, 2017, **784**, 55–61.
107 J. He, J. Sunarso, Y. Zhu, Y. Zhong, J. Miao, W. Zhou and Z. Shao, *Sens. Actuators, B*, 2017, **244**, 482–491.
108 R. Madhuvilakku, S. Alagar, R. Mariappan and S. Piraman, *Anal. Chim. Acta*, 2020, **1093**, 93–105.
109 L. Liu, J. Du, W. E. Liu, Y. Guo, G. Wu, W. Qi and X. Lu, *Anal. Bioanal. Chem.*, 2019, **411**, 2189–2200.
110 W. Zhang, J. Zheng, Z. Lin, L. Zhong, J. Shi, C. Wei, H. Zhang, A. Hao and S. Hu, *Anal. Methods*, 2015, **7**, 6089–6094.
111 L. A. D. Gugoasa, F. Pogacean, S. Kurbanoglu, L. Barbu-Tudoran, A. B. Serban, I. Kacso and S. M. Pruneanu, *J. Electrochem. Soc.*, 2021, **168**, 067523.
112 Y. Chen, X. Liu, S. Zhang, L. Yang, M. Liu, Y. Zhang and S. Yao, *Electrochim. Acta*, 2017, **231**, 677–685.
113 H. Wang, Y. Wang, S. Li and J. Qu, *Anal. Methods*, 2017, **9**, 338–344.
114 S. Hu, W. Zhang, J. Zheng, J. Shi, Z. Lin, L. Zhong, G. Cai, C. Wei, H. Zhang and A. Hao, *RSC Adv.*, 2015, **5**, 18615–18621.
115 S. Radhakrishnan, K. Krishnamoorthy, C. Sekar, J. Wilson and S. J. Kim, *Chem. Eng. J.*, 2015, **259**, 594–602.
116 J. Jiao, M. Pan, X. Liu, J. Liu, B. Li and Q. Chen, *Nanomaterials*, 2020, **10**, 499.
117 Y. Cui, J. Li, M. Liu, H. Tong, Z. Liu, J. Hu and D. Qian, *Microchim. Acta*, 2020, **187**, 589.
118 A. Mejri, A. Mars, H. Elfil and A. H. Hamzaoui, *Microchim. Acta*, 2019, **186**, 1–9.
119 J. Li, J. Jiang, D. Zhao, Z. Xu, M. Liu, P. Deng, X. Liu, C. Yang, D. Qian and H. Xie, *J. Alloys Compd.*, 2018, **769**, 566–575.
120 L. A. D. Gugoasa, R. I. Stefan-van Staden, J. F. van Staden, M. Coros and S. M. Pruneanu, *Anal. Bioanal. Chem.*, 2020, **412**, 5191–5202.
121 Y. Luo, Y. Wang, H. Yan, Y. Wu, C. Zhu, D. Du and Y. Lin, *Anal. Chim. Acta*, 2018, **1042**, 44–51.
122 R.-I. Stefan-Van Staden, L. A. Gugoasa, C. Socaci and A. R. Biris, *RSC Adv.*, 2015, **5**, 66185–66191.
123 R. I. Stefan-van Staden, R. M. Ilie-Mihai, L. A. Gugoasa, A. Bilasco, C. A. Visan and A. Streinu-Cercel, *Anal. Bioanal. Chem.*, 2018, **410**, 7723–7737.
124 Z. Qin, G. Ren, Q. Liu, X. Lu, Q. Zhang, A. Fan, Y. Lu, N. Li, X. Chen and D. Zhao, *J. Pharm. Biomed. Anal.*, 2018, **155**, 7–14.
125 L. A. D. Gugoasa, A. Baracu and G. Craciun, in *2021 Proceedings of the International Semiconductor Conference (CAS)*, IEEE, 2021, pp. 283–286.
126 J. Du, Y. Tao, J. Zhang, Z. Xiong, A. Xie, S. Luo, X. Li and C. Yao, *Mater. Technol.*, 2019, **34**, 665–673.
127 L. Sheng, Z. Li, A. Meng and Q. Xu, *Sens. Actuators, B*, 2018, **254**, 1206–1215.
128 H. Luo, Y. Y. Zhao, X. Y. Jin, J. M. Yang, H. Cong, Q. M. Ge, L. Sun, M. Liu and Z. Tao, *Electroanalysis*, 2020, **32**, 1449–1458.
129 N. Ross and N. Civilized Nqakala, *Anal. Lett.*, 2020, **53**, 2445–2464.
130 M. M. El-Wekil, M. Darweesh, M. S. A. Shaykoon and R. Ali, *Talanta*, 2020, **217**, 121084.
131 L. A. Dinu, S. Kurbanoglu, C. Romanitan, S. Pruneanu, A. Serban, M. Stoian, C. Pachiu and G. Craciun, *Appl. Surf. Sci.*, 2022, **604**, 154392.
132 N. Lu, Y. Liu, X. Yan, Z. Xu, Y. Xing, Y. Song, P. Zhao, M. Liu, Y. Gu, Z. Zhang and S. Zhai, *ACS Appl. Nano Mater.*, 2022, **5**, 11361–11370.
133 Y. Liu, P. Zhao, Y. Liang, Y. Chen, J. Pu, J. Wu, Y. Yang, Y. Ma, Z. Huang, H. Luo, D. Huo and C. Hou, *Talanta*, 2023, **254**, 124171.
134 X. Chen, X. J. Huang, L. G. Kong, Z. Guo, X. C. Fu, M. Q. Li and J. H. Liu, *J. Mater. Chem.*, 2010, 352–359.
135 L. Pan, J. Tang and Y. H. Chen, *Sci. China: Chem.*, 2013, **56**, 362–369.
136 T. Abdiryim, A. Ali, R. Jamal, Y. Osman and Y. Zhang, *Nanoscale Res. Lett.*, 2014, **9**, 1–8.
137 J. E. Choe, M. S. Ahmed and S. Jeon, *J. Electrochem. Soc.*, 2016, **163**, B113–B118.
138 H. Jia, J. Xu, L. Lu, Y. Yu, Y. Zuo, Q. Tian and P. Li, *Sens. Actuators, B*, 2018, **260**, 990–997.
139 S. Dang, Q. L. Zhu and Q. Xu, *Nat. Rev. Mater.*, 2018, **3**, 17075.
140 Z. Zhou, F. Liu, Y. Huang, Z. Wang and G. Li, *Int. J. Biol. Macromol.*, 2015, **77**, 336–343.
141 Z. Wang, X. Li, H. Liang, J. Ning, Z. Zhou and G. Li, *Mater. Sci. Eng., C*, 2017, **79**, 227–236.
142 Y. Zheng, A. Wang, W. Cai, Z. Wang, F. Peng, Z. Liu and L. Fu, *Enzyme Microb. Technol.*, 2016, **95**, 112–117.
143 C. Gao, X. Y. Yu, R. X. Xu, J. H. Liu and X. J. Huang, *ACS Appl. Mater. Interfaces*, 2012, **4**, 4672–4682.
144 J. T. Mefford, X. Rong, A. M. Abakumov, W. G. Hardin, S. Dai, A. M. Kolpak, K. P. Johnston and K. J. Stevenson, *Nat. Commun.*, 2016, **7**, 11053.
145 H. Jiang, D. Zhang, Z. He, Q. Lian, Z. Xue, X. Zhou and X. Lu, *Anal. Lett.*, 2015, **48**, 1426–1436.
146 E. Ko, V. K. Tran, S. E. Son, W. Hur, H. Choi and G. H. Seong, *Sens. Actuators, B*, 2019, **294**, 166–176.
147 H. Mao, M. Liu, Z. Cao, C. Ji, Y. Sun, D. Liu, S. Wu, Y. Zhang and X. M. Song, *Appl. Surf. Sci.*, 2017, **420**, 594–605.
148 V. Stanković, S. Đurđić, M. Ognjanović, J. Mutić, K. Kalcher and D. M. Stanković, *J. Electroanal. Chem.*, 2020, **876**, 2–7.
149 V. Suvina, T. Kokulnathan, T. J. Wang and R. G. Balakrishna, *Microchim. Acta*, 2020, **187**, 189.

150 J. Balamurugan, T. D. Thanh, G. Karthikeyan, N. H. Kim and J. H. Lee, *Biosens. Bioelectron.*, 2017, **89**, 970–977.
151 Y. Fu, D. Huang, C. Li, L. Zou and B. Ye, *Anal. Chim. Acta*, 2018, **1014**, 10–18.
152 H. Yang, J. Bao, Y. Qi, J. Y. Zhao, Y. Hu, W. Wu, X. Wu, D. Zhong, D. Huo and C. Hou, *Anal. Chim. Acta*, 2020, **1135**, 12–19.
153 N. Shishegari, A. Sabahi, F. Manteghi, A. Ghaffarinejad and Z. Tehrani, *J. Electroanal. Chem.*, 2020, **871**, 114285.
154 D. Yin, X. Bo, J. Liu and L. Guo, *Anal. Chim. Acta*, 2018, **1038**, 11–20.
155 Z. Lu, L. Wu, J. Zhang, W. Dai, G. Mo and J. Ye, *Mater. Sci. Eng., C*, 2019, **102**, 708–717.
156 B. Hou, H. Liu, S. Qi, Y. Zhu, B. Zhou, X. Jiang and L. Zhu, *J. Colloid Interface Sci.*, 2018, **510**, 103–110.
157 U. Rajaji, M. Govindasamy, S. M. Chen, T. W. Chen, X. Liu and S. Chinnapaiyan, *Composites, Part B*, 2018, **152**, 220–230.
158 W. Huang, Y. Xu and Y. Sun, *Front. Chem.*, 2022, **10**, 873187.
159 W. Xue, X. Bo, M. Zhou and L. Guo, *J. Electroanal. Chem.*, 2016, **781**, 204–211.
160 S. Samuei, J. Fakkar, Z. Rezvani, A. Shomali and B. Habibi, *Anal. Biochem.*, 2017, **521**, 31–39.
161 K. K. Naik, A. Gangan, B. Chakraborty, S. K. Nayak and C. S. Rout, *ACS Appl. Mater. Interfaces*, 2017, **9**, 23894–23903.